MASTER THESIS

The effect of osmotic pressure on the mechanical and structural properties of individual collagen fibrils

Submitted in partial fulfillment of the requirements
for the academic degree of Master, under supervision of

Dr. Orestis ANDRIOTIS
Prof. Philipp J. THURNER

at

Institute of Lightweight Design and Structural Biomechanics - E317,
Vienna University of Technology

by

Sylvia Desissaire
Matr.Nr. 1428115

Vienna, on 01.2016 _____

Abstract

Collagen fibrils are one of the main building blocks of the human body at the nanoscale. They are present in many different tissues such as lungs, cartilage, bones or tendons. They are of a great biomechanical importance providing structural and mechanical stability and constitute the framework in which cells reside and function. In many tissues, if not all, collagen fibrils co-exist with proteoglycans, which are located in the interfibrillar space of the extra cellular matrix and bear high negative charges at physiological pH. These negative charges create a cation (salt ions) concentration gradient and as a result exert osmotic pressure on collagen fibrils. Although, proteoglycans seem to play a significant role in tissues such as tendon and cartilage, the effect of osmotic pressure on the structural and mechanical properties of individual collagen fibril is largely unknown. The aim of this master thesis project is thus to investigate the effects of increasing osmotic pressure on individual collagen fibrils.

Atomic force microscopy (AFM) allows for direct evaluation of both the mechanics and the structure of individual collagen fibrils at the nanoscale level. In this study, AFM was used to image, indent and pull individual collagen fibrils. Firstly, imaging and cantilever-based nanoindentation experiments on individual collagen fibrils in air, phosphate buffered saline (PBS) and solutions of increasing concentration of polyethylene glycol (PEG) were performed. Solutions of increasing concentration of PEG were used to create varying osmotic pressures, *in situ*, during measurements. Then a protocol was developed to perform nanotensile experiments on individual collagen fibrils using the AFM. Finally, these experiments were performed on individual collagen fibrils in PBS and solutions of increasing concentration of PEG. These experiments aimed to generate a relationship linking osmotic pressure to collagen fibril mechanics.

Collagen fibrils shrink and become stiffer with increasing osmotic pressure. The fibril diameter reduces up to 15%-20% at the highest PEG concentration used (solution in 3.5M PEG). Nanoindentation experiments provide information about the transverse elastic modulus which increases 44 times from PBS to a solution of 3.5M PEG in PBS. The longitudinal elastic modulus is obtained from the nanotensile experiments and increases by a factor of 3 at 3.5M PEG. Mechanical conditioning of an individual collagen fibril was highlighted with softening of the fibril under cycling loading. It is demonstrated all along this study that osmotic pressure is a major contributor to the function of collagen fibrils. The main take home message being that the structural and mechanical properties of individual collagen fibrils can finely be tuned to a high range using osmotic pressure.

Further experiments and analysis are required to fully understand the consequences of osmotic pressure on individual collagen fibril. Influence of the osmotic pressure on the mechanical conditioning is also not well determined. Understanding how, from similar main building blocks (i.e. the collagen fibrils), the properties of tissues can be adapted to assume numerous distinct functions is one of the futures challenges. For example, cells might be reducing or increasing the amount of proteoglycans to tune the mechanical properties of their microenvironment i.e. of near by collagen fibrils.

Acknowledgements

I would like to sincerely thank all the members of the Institute of Lightweight Design and Structural Biomechanics and all the people who helped me throughout this master thesis.
This work could have particularly not be done without the wise advices of my supervisors Dr Orestis Andriotis and Prof Philipp Thurner to whom I express all my gratitude.

Contents

List of Figures

Chapter 1

Introduction

1.1 Background and motivation

Connective tissues are composed of cells and the extracellular matrix (ECM). The ECM includes water and a large variety of macromolecules, which are mainly collagen, elastin, proteoglycans and glycosaminoglycans. In mammals, collagen is the most abundant protein (macromolecules composed of one or more chains or amino acids). It is present in a large variety of body structures such as bones, tendons and skin. Its primary role is to provide structural and mechanical stability to the tissues. It is characterized by its high strength and stiffness in tension. The composition and organization of collagen-based tissues can change to satisfy specific mechanical requirements according to the loading conditions and the targeted function [6]. Decline of tissue functionality can however be observed through changes in the mechanical properties at the macroscale level [7]. Due to its excellent biocompatibility, biodegradability and weak antigenicity, collagen is also one of the most useful biomaterials. Tissue engineering (as skin replacement, bone substitute) or drug delivery systems are examples of the many possible medical applications [8]. Methods improving the understanding of the structure-mechanical relationship at the smallest level of human body structures would, in particular, increase precision and accuracy in medical applications. It would also enhance the comprehension of the changes of collagen mechanics in diseases or due to inflammatory disorders.

Type I collagen is the most abundant collagen protein in the human body. It self assembles into large fibrillar structures with diameters ranging from 30 nm to 500 nm [9]. For the last decade, analysis methods such as scanning electron microscopy (SEM) or atomic force microscopy (AFM) have been used to investigate collagen fibrils. AFM nanoindentation gives nanomechanical results that where not accessible with conventional macroscopic technique tools. Such macroscopic techniques are indeed based on direct manipulation and visual observation which are not easily applicable to nanoscale dimensions [10]. The measurements from AFM nanoindentation are used to link mechanical properties from the nanoscale to the macroscale. They also facilitate modeling and implementation of theoretical models, where unknown mechanical or structural properties, due to the lack of data, often are coarsely estimated. In tissue biomechanics, tensile tests are widely used to obtain parameters such as stiffness, toughness and strength. Collagen fibrils are in particular characterized by their stress-strain responses, but they are only a few datasets in literature [11]. Comprehension of collagen fibril assembly and mechanical properties at the nanoscale level is, however, a topic of ongoing research.

One basic question is concerned with the impact of the biochemistry, i.e. of the cross-links, and the chemical environment, i.e. of the osmotic pressure in the ECM, on collagen fibril mechanics. Such parameters can be controlled by cells. On the one hand, cross-links are slowly established in tissues to create an interconnected fibrillar material. Several studies have highlighted their importance in tuning mechanical properties such as toughness and strength [6], [12]. On the other hand, osmotic pressure in the ECM is a main contributor of balancing external pressures and contributes to the viscoelastic characteristics of soft tissues under deformation [13]. The ECM is in particular constituted of water, proteoglycans and glycosaminoglycans, main actors of the osmosis. In tendons, interactions between water and collagen fibrils in the load-carrying environment are not fully understood [14]. Responses of collagen molecules upon water removal have been recently investigated. Changes in their conformation are observed under osmotic pressure [14]. For this reason, the importance of osmotic pressure on collagen fibrils can not be neglected. Osmotic pressure may indeed be one main contributor to the collagen fibrils responses to load. Focusing on how collagen fibrils react to osmotic pressure may enhance comprehension of how cells can, much quicker than through enzymatic cross-links, tune their mechanical environment.

1.2 Importance of collagen in human body

Collagen composes about 25% of the total protein mass found in the human body. This protein is essential for many organs such as the respiratory system, bones, cartilage or ligaments and tendons. Collagen molecules self assembled into larger organized cylindrical structures: the collagen fibrils. These are in turn organized in fibres to form organs at the tissue level. Structure, with collagen as a basic building block, is highly correlated to function, that is mechanical properties. Collagen thus is of a great biomechanical importance for both hard tissues and soft tissues.

The dynamic interactions between cells and collagen regulates tissue remodelling during growth, differentiation, wound healing and morphogenesis [5]. In bones, the interactions between the mineralized collagen fibrils and the matrix of mineralized noncollagenous proteins provide its characteristic properties, stiffness and toughness, in order to protect vital internal organs [15], [16]. In tendons and ligaments, the interactions between collagen fibrils and proteoglycans allow to increase ductility and energy storage and are in particular facilitating motion [17]. In lungs, the interactions between collagen fibrils and proteoglycans stabilize the collagen-elastin network and contribute to lung elasticity and alveolar stability [18]. These are only few examples of the many roles of collagen, an essential protein of the human body.

1.3 Thesis goal

The high number of negative charges carried by proteoglycans create a cation concentration gradient and as a result exert osmotic pressure on collagen fibrils by attracting ions and water from them. This effect, present in all tissues, is not studied to large extent and the consequences of such pressure on the structural and mechanical properties of fibrils has little been studied. Atomic force microscopy (AFM) allows both structural and mechanical assessment of collagen fibrils at the nanometer scale and can be employed to

assess the effect of proteoglycans on the structure and mechanics of individual collagen fibrils. The aims of this thesis are:

(a) Perform AFM imaging and cantilever-based nanoindentation on individual collagen fibrils in liquid, with increasing concentrations of a negative charged molecule (polyethylene glycol; PEG), i.e. at increasing osmotic pressures.

(b) Develop an experimental protocol and perform nanotensile tests in liquid using the AFM on single fibrils under increasing osmotic pressure to derive force-distance and stress-strain curves and assess variation in stiffness.

(c) Deduce a relationship linking osmotic pressure to fibril structure and mechanics.

1.4 Structure of the thesis

Chapter 2 introduces the structure, the roles and main properties of collagen fibrils and collagen-based tissues. The notion of osmotic pressure from a theorical point of view as well as its effect at the collagen fibril level is presented at the end of the chapter.

Chapter 3 is dedicated to AFM, explaining the main components of the instrument used as well as the basic imaging modes and the feedback loop.

Chapter 4 describes the materials and methods of the experiments conducted. Protocols of the AFM cantilever-based nanoindentation and nanotensile tests are presented. Analysis methods chosen are also included in this chapter.

Chapter 5 is concerned with the results of the experiments. Influences of increasing osmotic pressure on the structure and mechanics of individual collagen fibrils are presented.

Finally, in chapter 6 discussion and conclusion of the master thesis work is given. The experimental outcomes are compared to the current literature. Limitations and further development are discussed. Further, a clear summary of the thesis outcomes is presented.

Chapter 2

Collagen in the human body

The human body of an adult human is composed of 60-70% of water. Proteins are the second main component, representing approximately 20%. Collagen composes 35% of the total protein mass found in the human body. We can find over 25 collagen types from 30 specific collagen genes [19] and collagen type I is the most abundant and the major organic constituent of tendons, bones and dentin. Collagen fibrils are perhaps one of the most important building blocks of most, if not all, biological tissues. Without them, our body would not be able to maintain itself and our muscles would not be able to function.

2.1 Hierarchical structure of collagen tissues from macroscale to nanoscale

Each tissue follows different and precise organizations at different length scale levels. Collagen fibrils used within this master thesis were obtained from mouse tendon. The organization of tendons from macroscale to nanoscale is described below (see Figure: 2.1) .

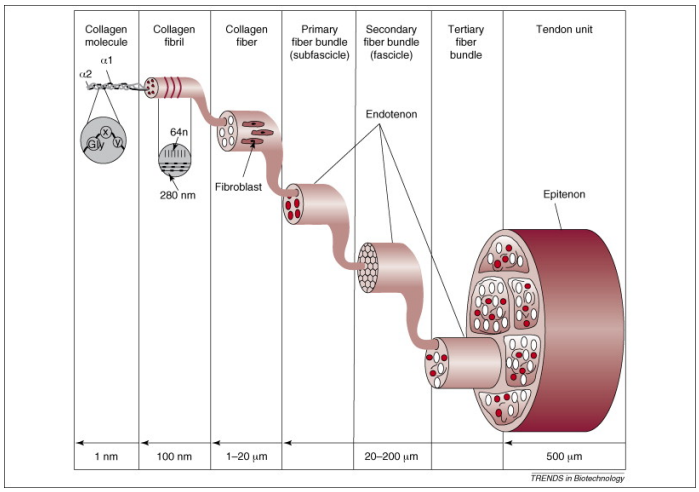

Figure 2.1: Schematic illustration of the hierarchical structure of tendon [1]

Tendons connect muscles to bones and transmit the mechanical force between them. They exhibit one of the highest strengths among the other soft tissues. Tendons themselves are composed of collagen (mostly type I) and elastin embedded in a proteoglycan-water matrix.

Collagen represents approximately 65% to 85% of dry mass of tendon, while elastin is about 1% to 2% of it [1] . They generally are surrounded by a loose aerolar connective tissue (paratendon) mainly made of an assembly of collagen type I and III and elastic fibrils. Under this layer can be found the epitendon, thin layer that sheaths the tendon unit.

The first biggest unit making up tendons are the tertiary fibers bundles. These are made of secondary fiber bundles in turn. Secondary fiber bundles are called fascicles. These units are made of collagen fibers: the primary fiber bundle (subfascicle). These three layers (i.e. first, second and third fiber bundles) are surrounded by a sheath of connective tissue (endotendon) participating to the gliding of bundles against one another during movement. The next unit are the collagen fibers. Their number and their diameter in each primary bundle vary from one tendon to another ([20] , [21]). The diameter in rat tail tendon ranges between 5 μm to 30 μm while in human tendon the diameter can be around 300 μm. They are composed of an assembly of collagen fibrils held together by cross links and a hydrated proteoglycan-rich matrix. The diameter of collagen fibrils varies between 20 nm to 500 nm and several tenths of μm in length. Collagen fibrils form due to a self assembly process of hydrated tropocollagen molecules. Theses molecules consist of three collagen polypeptide chains which are 2 α1-type I and 1 α2-type I chains for collagen type I. The tropocollagen molecule is composed of a helical domain and two non-helical domains named telopeptides, located at the two ends of the molecule. Collagen fibrils can be recognized by the periodic D-banding of about 67 μm of the collagen molecules (see Figure: 2.2). The D-periodicity has been initially explained by the Hodge-Petruska model ([22]), which is a simplified 2D arrangement of five tropocollagen molecules with a slight offset resulting in the gap (low density) and overlap regions (high density).

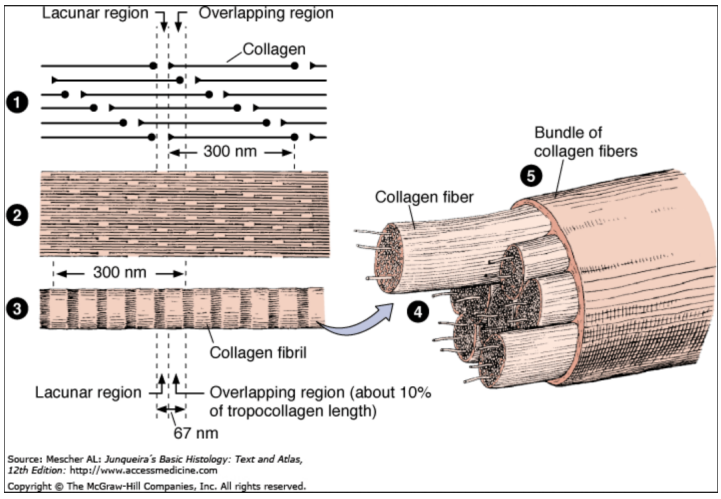

Figure 2.2: Schematic illustration of collagen arrangement in fibrils

At the collagen molecule level shown in Figure 2.2 are the tropocollagen molecules described before:

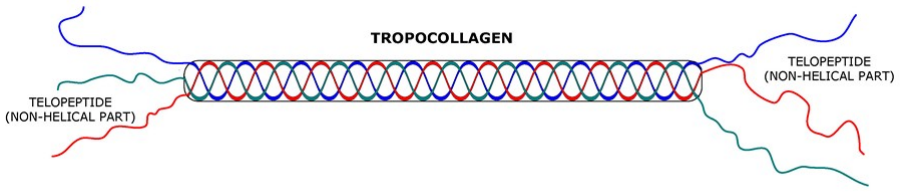

Figure 2.3: Schematic illustration of a tropocollagen molecule (from eanovacoll website)

2.2 General properties of collagen fibrils and collagen-based tissues

Different biological tissues have different mechanical properties, i.e. strength, stiffness and toughness, which highly depend on the structural components and their arrangement at the lowest hierarchical length scale level. Stiffness defines how a material resist to deformation. A strong material needs a large force to break and its corresponding strength is then the maximum stress reached before breaking. The toughness is the total energy needed to break a material. As an example, the elastic modulus of collagen fibrils is estimated to range between 1.25 MPa and 25 GPa when including mineralized collagen [7]. When considering only individual type I collagen fibril from rat tail, the reduced elastic modulus was found to be between 5 GPa and 11.5 GPa in air and at room temperature. Measurements were done by AFM nanoindentation [23]. When giving and interpreting values for collagen fibril properties, nature of the connective tissue considered has to be precised. Mechanical properties may also depend on the local architecture and mechanical needs, according to the environment. They can thus differ through a tissue and it is then essential to remember not to consider them as constant values. Human to human variability should also be taken into account. Biological response to a mechanical stimuli controls the adaptation of tissues to specific conditions and enables damage repair.

Collagen fibrils are assembled into composite materials. Complexity and properties of such structures are function of fibers arrangement leading to anisotropic properties. Mechanical properties of such collagen-based tissues are thus dependent of the direction considered. Fibrous tissues are stronger in fibers direction than perpendicular to it. Changing fibers assembly gives the possibility to achieve a wide range of properties. As an example, orientation of collagen fibers in human femur is not random, but correlated to the tensile and compressive stresses (see Figure: 2.4). Regions carrying tensile stresses have more longitudinally oriented fibers while the one carrying compressive stresses have more transversely oriented ones [24].

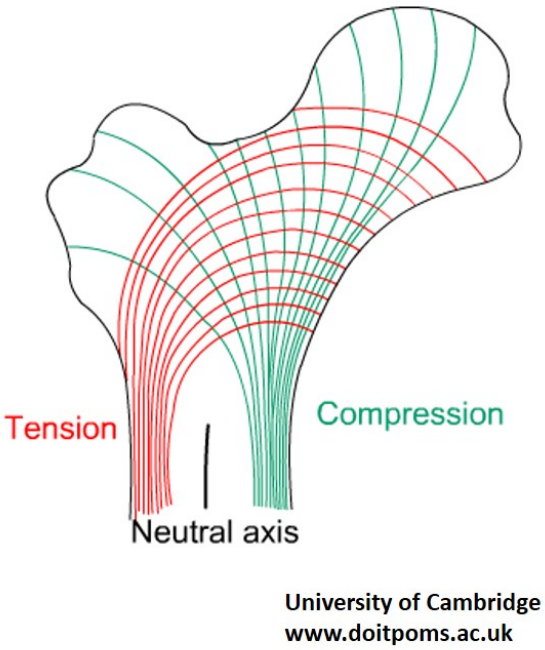

Figure 2.4: Trabecular bone architecture aligned with principal stresses in human femur

2.3 Collagen cross-linking

Biological response and mechanical behavior are much more determined by this internal architecture than by the chemical composition itself. Cells enable the slow modification of the biochemistry of collagen fibrils by cross-links. Collagen fibril cross-links and interaction with the ECM enhance the development of the required characteristics. The resulting stress-strain curves are significantly different, as we can see for bones and tendons. The curve obtained from the bone sample has a higher Young's modulus representing of the stiffer behavior of the bone (see figure 2.5). This one is also more brittle with a widely smaller strain before breaking compare to the tendon. In a simplified manner, this can be explained by the mineralized composition while the collagen fibers are responsible for the toughness of bone.

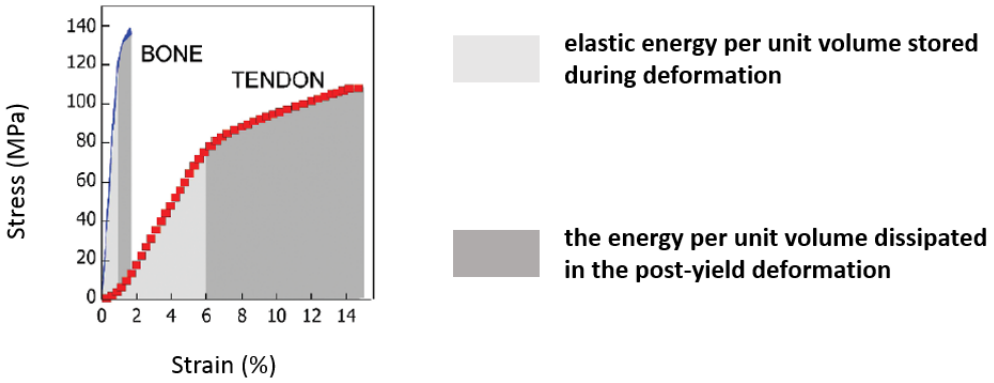

Figure 2.5: Stress-strain curves for mouse tail tendon (Misof et al. 1997 [2]) and for parallel fibered bone (Gupta et al. 2006 [3])

Collagen cross-links can be divided in two main types according to their origin of formation: the enzymatic cross-links and the non-enzymatic cross-links.

2.3.1 Enzymatic cross-links

Enzymatic cross-links are the first formed during the fibrillar assembly. They ensure a stabilized structure of the newly synthesized collagen fibril [25]. Enzymes, such as the lysyl oxidase and hydroxylase, initiate the process leading to cross-links between lysine and hydroxylysine residues located at the telopeptides. First, immature, divalent, cross-links are formed between the helical domain and non-helical domain of two adjacent molecules. Due to chemical reactions, trivalent cross-links are then formed. There are qualified of mature cross-links, connecting a third collagen molecule.

2.3.2 Non-enzymatic cross-links

Non-enzymatic cross-links are established later in the collagen fibril formation than the enzymatic cross-links. They result from instantaneous chemical reactions between collagen and glucose [5]. Oxidation leads to the formation of advanced glycation end products (AGEs) that link two helical domains of adjacent molecules.

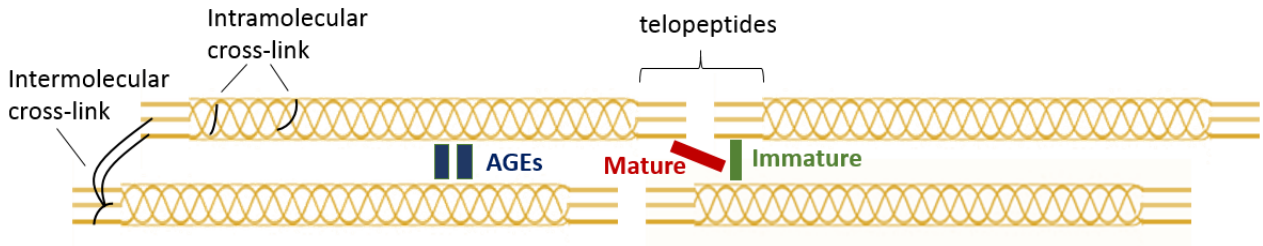

Figure 2.6: Schematic illustration of immature, mature and AGEs cross-links

2.4 Osmotic pressure on collagen fibrils

2.4.1 Notion of osmotic pressure

Osmosis is the transfer of a solvent through a semi-permeable membrane under the action of a concentration gradient. A semi-permeable membrane is defined as a membrane allowing diffusion of the solvent but not the solutes. The solvent flow goes from a region of lower concentration, dilute solution, to one of higher concentration, concentrated solution. A dilution of the concentrated solution is obtained. The existence of such a flow indicates that the system is not in an equilibrium state. Equilibrium can be reached again by applying a hydrostatic pressure in order to cancel the flow of solvent. The osmotic pressure is then defined as the hydrostatic pressure exerted on the solution to prevent the solvent from crossing the semi-permeable membrane [26] .
Different types of osmometers exist: vapor pressure depression osmometer, freezing point depression osmometer and membrane osmometer. Freezing point depression osmometers are frequently used in Clinical Chemistry Labs and Quality Control Labs. We will however explain the principle of a membrane osmometer to illustrate how does osmosis work. It is used to determine the average molecular weight (Mn) and is made as below (see Figure 2.7): a semipermeable membrane separates two chambers. One is the solvent chamber closed to the atmosphere while the second one is the solute chamber open to the atmosphere. Since the chemical potential of the solvent is much higher than that of the solute, the solvent flows through the membrane and reaches the solute chamber, where it diffuses due to the difference of concentration. The pressure of the solvent starts decreasing with the flow. When the pressure difference across the membrane counteracts the chemical potential difference caused by the solute, equilibrium is reached: this pressure difference is defined as osmotic pressure.

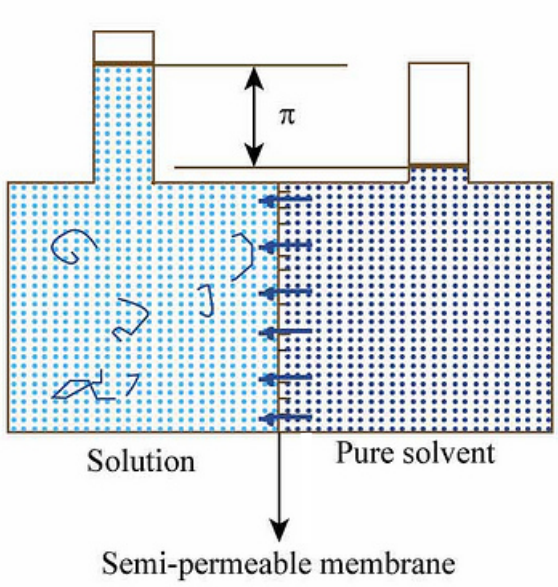

Figure 2.7: Schematic illustration of the principle of an osmometer

The law of Vant' Hoff is expressed as:

$$\pi = RT\frac{C}{M} \tag{2.1}$$

with π the osmotic pressure in Pa, C the weight concentration of solute, M the molar mass, T the absolute temperature and R the ideal gas constant. Two conditions need to be satisfied to apply this law:

- the osmometer membrane is strictly permeable, only water can flow through,
- Solutions are diluted.

At the collagen fibril level, the semi-permeable membrane is represented by the surface of the fibril. When swelling occurs, water and ions come into the fibril and increase the lateral separation distance between the collagen molecules. The two chambers are the ECM and the fibril itself.

2.4.2 Collagen fibrils interact with proteoglycans

Fibrils are joint to a peripheral matrix rich in proteoglycans which bear highly negative charges at physiological pH. Proteoglycans affect the collagen assembly and contribute to the mechanical behavior of the tissue. As an example decorin or fibromodulin delay the collagen fibril assembly, which seem to usually result in a reduction of fibril diameter [19]. Depending on the proteoglycans considered, different contribution and biological effects could be observed and are independent of their effects on collagen assembly [19] . In tendons, proteoglycans increase toughness and permit the storage of energy during loading. As a consequence, this facilitates motion [5]. Proteoglycans allow inter-fibrillar sliding during tensile loading as it is show on Figure 2.8.

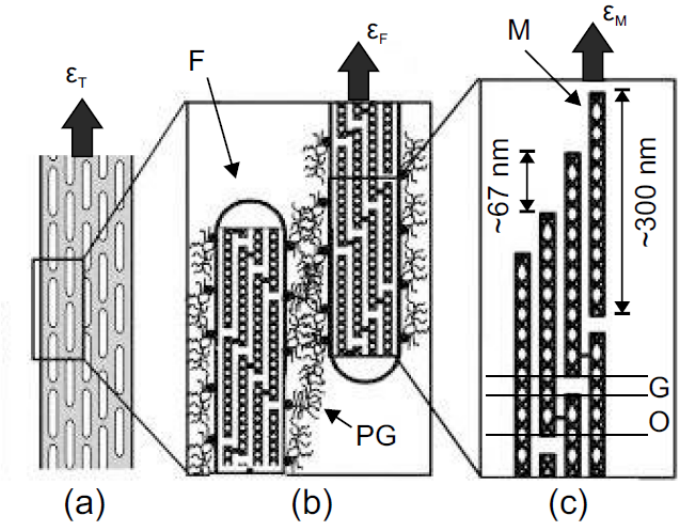

Figure 2.8: Schematic illustrations of tendon fascicle during loading at different scales with ϵ_t the tissue strain, ϵ_f the fibril strain and ϵ_m the molecular strain. (F: fibril and PG: proteoglycans) [4]

The individual mechanical properties of the tissue components, as collagen or proteoglycans, and their interactions with each other at the nanoscale determine to a large amount the mechanical function of this tissue at the macroscale [5]. Osmotic pressure is controlled by the amount of proteoglycans, i.e. the amount of negative charges. Consequences of such a pressure on collagen fibrils can be studied thanks to in vitro tests [14]. However, it is not known yet how osmotic pressure is able to tune collagen structural and mechanical properties.

2.5 Tensile properties of individual collagen fibrils under physiological conditions

Recent studies have investigated the tensile properties of individual collagen fibrils using different experimental methods. Microelectromechanical systems platforms can, in particular, be used in order to obtain reproducible measurements of mechanical properties of individual collagen fibrils under cyclic loading. Stress-strain curves are plotted from the experimental data. At small strain, linear behavior with an elastic modulus of 0.86 $\pm$0.45 GPa was reported for individual partially hydrated collagen fibril [11]. Under cyclic loading, unloading curves appear to be steeper than the initial loading curve resulting in residual strains. The initial condition can substantially be recovered by applying a prolonged resting time in a humid environment. Mechanisms involved in such a recovery are not well defined, but may probably result from intramolecular and intermolecular relaxation of the collagen molecules. Atomic force microscopy can also be used to perform cyclic testing. Experiments were repeatedly done in phosphate buffered saline (PBS) in the pre-yield region at different strain rates. The elastic stress-strain response can be fitted with a second order polynomial function, while the viscous response is linear [27]. The elastic component is the zero-rate stress relaxation. The viscous component is then calculated by extraction the elastic part from the dynamic curves resulting of the experiments. The slope of the viscous response shows a strain rate dependence and is respectively 0.242 and 0.168 for the two fibrils of the study [27]. An increase in strain rate results in an increase in stress at a same strain. Providing a range of values for the longitudinal elastic modulus of an individual collagen fibril is complicated since many parameters are involved. Indeed, the results may vary with the experimental environment as well as with the strain rate and the relaxation time. The yield strength was found to be around 0.22 $\pm$0.14 GPa [11]. However, its value is difficult to determine, in part due to the same previously mentioned reasons, and may be altered by the inaccuracies of the experimental process at the nanoscale. It seems that at the first loading, the fibrils may be able to sustain higher stress, of about 0.47GPa, without yielding. Cyclic loading can cause an accumulation of damages in the fibril. Moreover, some fibrils are experiencing brittle rupture at their edges that may likely result from stress concentrations at the edge of the fibril-epoxy interface.

Theoretical and molecular modeling had also been developed to understand the nanostructure of the collagen fibrils and their response to load. The Buehler model predicted a yield strength of about 0.3 to 0.4 GPa for uncross-linked fibril [28]. In this model, the length of tropocollagen molecules and the strength of intermolecular interactions are found to play a determinant role in the deformation mechanics. Long molecules make the collagen fibrils more robust with significant energy dissipation. Cross-links are providing additional strength to the fibril but can also make the fibril more brittle. The model shows that both the elastic strength and the energy dissipation approach a finite value for large molecular lengths. Thus, having tropocollagen molecules longer than about a few hundred nanometers would be inefficient [28]. This agrees with the tropocollagen length of about 300 nm found in different experiments [29], [30]. However, this model is a material model and not a structural one, meaning it contains no intrinsic diameter. Experimental studies show that mechanical properties are dependent of the collagen fibril geometry [11]. As the volume of the fibril increases, the yield strength decreases and values obtained are smaller than the one predicted by the Buehler model. Structural inhomogeneities would

add stress concentrations leading to a smaller yield strength.

As structural changes seem to tune the mechanical properties of collagen fibril, experiments were carried on in order to compare the structural and mechanical answers of an individual collagen fibril in a dry state and in an hydrated one [31], [14]. The collagen fibril swells when hydrated: water molecules are driven in the fibril due to the osmotic pressure applied. From the hydrated state to the dry one, the collagen fibrils are conversely shrinking in width. This shrinkage was found to be in between 1.3% and 2.5% depending on the fibrils [14]. Such results suggest that water is playing an essential role in tuning the structure of collagen fibrils. In parallel, the effects of the osmotic pressure on the mechanical properties such as the transverse elastic modulus of the fibril were also investigates. Under complete dehydration, very large stress, up to 100 MPa, are generated and the transverse elastic modulus significantly increases. Such stresses are resulting from the molecular and supramolecular changes. Smaller changes in the osmotic pressure level in the range of the osmotic pressure exerted by proteoglycans, i.e 0.4 MPa should also produce macroscopic stresses [14]. The water-generated tensile stresses, i.e. the water-mediated hydrogen bonding, may be essential to ensure the role of collagen-based tissues. They seem to dominate the tropocollagen interactions whereas Van der Waals and electrostatic effects are negligible [32]. Under cyclic loading, strain hardening and recovery may also result from the movement of water molecules in the system. When loading, the fibril is under tension, its radius is decreasing and water could be driven out the fibril under the pressure exerted. The fibril would, in this situation, become stiffer. When unloading, the fibril is able to extend again and water would be able to come back into the fibril causing recovery after a certain time [11]. Considering the results of these current studies, water is an active part of the protein unit and is stabilizing the structure of the collagen molecule.

Collagen is subjected to osmotic pressure under physiological conditions, which makes it particularly important to study. Most extracellular tissues are indeed typically presenting proteoglycans with collagen. For the last decade, experiments on collagen fibrils were done in solutions of different salt concentrations. However, the amount of results is still limited and can be contradictory. Longitudinal elastic modulus was found to considerably increase when salt is added in some results [31] while it was found insensitive to the environmental salt concentration in other results [33]. Such differences can be an effect of the solution used as well as the maximum concentration tested. The pH of the solution used for the experiments can also affect the results. At lower pH, ion pair interactions would seem to dominate over the hydration forces. Mimicking the physiological environment in which the collagen fibrils are developing themselves to reproduce the impact of the amount of proteoglycans is not easy. Investigations and results on the subject being limited, this is a reason why the experiments developed in this master thesis were carried out.

Chapter 3

Atomic force microscopy

3.1 Atomic force microscope

3.1.1 General principle

The atomic force microscope is part of a larger family of microscopes known as the scanning probe microscopes (SPMs). They differ from the conventional light microscopes by resolving the surface of a specimen by mechanical properties or interaction rather than optical or electromagnetic. SMPs technique is based on the use of a very sharp probe to scan a region of interest. The interaction between the surface and the probe are measured and changes in the magnitude of interaction between the probe tip and the surface scanned produce SMPs images. Resolution therefore depends on the tip apex sharpness (measured by the radius of curvature), the aspect ratio of the whole tip as well as the positioning accuracy of the scanner as presented on the Figure 2.7 below. The AFM uses a cantilever and its tip can be used, beyond resolving the structure, to obtain information of the mechanical properties. The cantilever can also be used to test samples under tensile forces. Another interesting advantage is its versatility, which enables to conduct experiments in air or aqueous environments as it had been done for the experiments of this thesis described later.

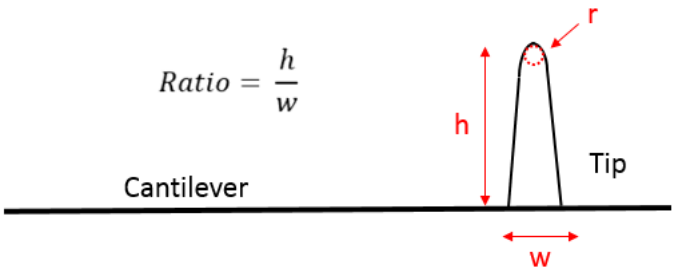

Figure 3.1: Schematic illustration of a tip and its parameters

The main compartments of an AFM are the cantilever and the tip, the piezoelectric transducers, and the components of the detection method.

3.1.2 The AFM cantilever and the tip

Cantilevers are microfabricated structures found in a number of geometry features, the most common ones being rectangular and triangular. AFM cantilevers are characterized by the spring constant, in other terms their stiffness, usually determined by their resonance frequency. Stiffness values can vary from 0.006 N/m to 85 N/m depending on the geometry [5]. Probing of softer surfaces can be accomplished using softer cantilevers in order to be sensitive enough to small changes of forces. And hence, the stiffer a sample is the stiffer the cantilever is to be used. This is even more important when performing mechanical tests with AFM. During mechanical tests, the true deformation of the sample to a certain load is wanted. Deformation is obtained by the deflection of the cantilever (see Figure 3.4): displacement is given by the Z-piezo movement minus the deflection. If a very soft cantilever is used to mechanically assess a very stiff sample, then the deflection of the cantilever over the sample may cause no or minute deformation of the sample. Hence, the sensitivity of the system is not appropriate and true sample deformation will not be accurately defined.
The AFM tip is a sharp spike microfabricated on the edge of the AFM cantilever (see Figure 3.2). They vary in geometry and size, the standard tip being a 3 μm tall pyramid with an end radius of about 5 to 10 nm.

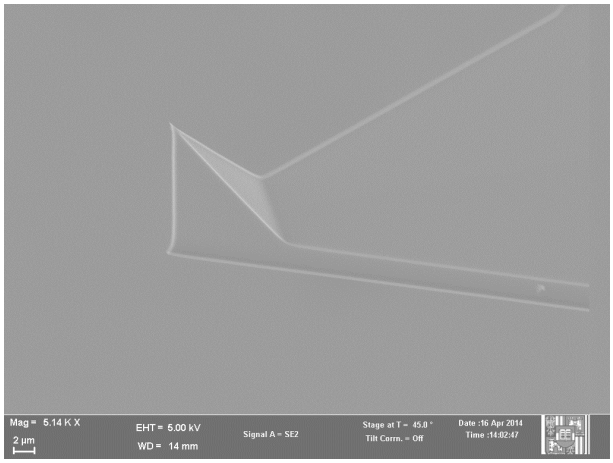

Figure 3.2: Example of an pyramid type AFM tip
(AC2OO, Olympus, tip radius: 7 nm)

Tip height however ranges from 3 μm to about 20 μm and tip radius from 5 nm to 100 nm [5]. These geometrical parameters of the tip can affect the imaging and can result to imaging artifacts. One of the most common artifacts during AFM imaging is the envelope effect [34]. The envelope effect results from the pyramidal shape of the tip during lateral scanning of the sample. When imaging collagen fibrils, recording the height and not the width is for this reason more accurate. Values for width will indeed be overestimated according to the tip shape.

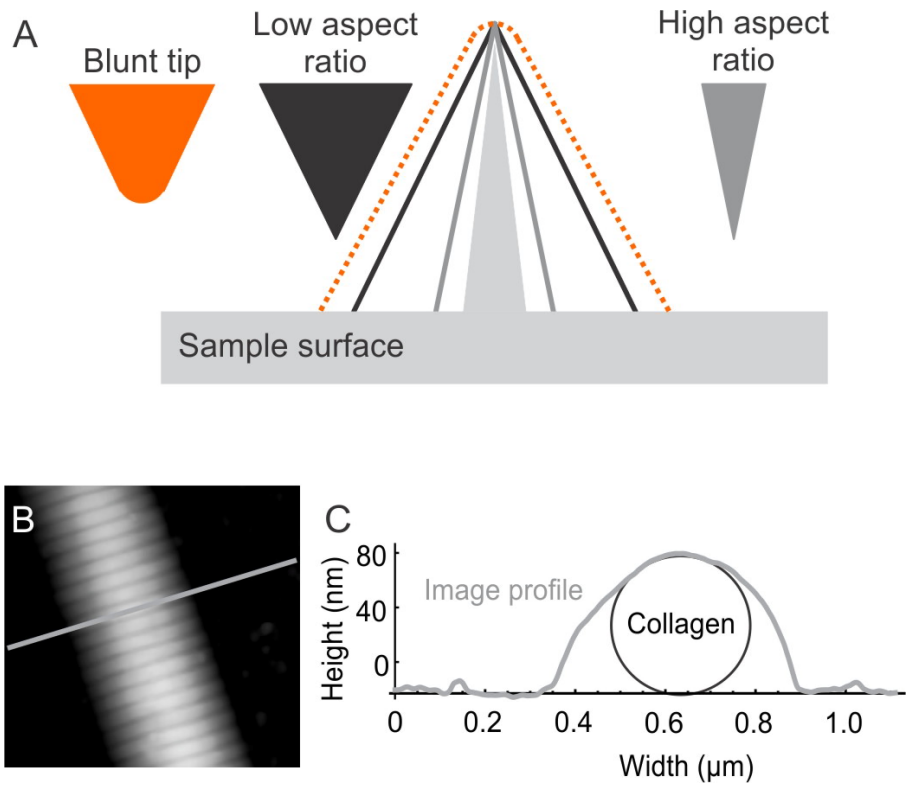

Figure 3.3: (A) Trace resulting from different tips
(B) AFM height image of a collagen type I fibril from wild type mouse tail tendon
(C) Corresponding profile of the cross section of the fibril compare to a perfect circle of the supposed fibril diameter
Adapted from O. Andriotis (2013) [5] with permission

3.1.3 The piezoelectric transducers

AFM actuators are made from a piezoelectric material. A piezoelectric actuator expands and retracts proportionally to an applied voltage. The piezoelectric effect relies on the generation of a potential across opposite faces of a non-conductive crystal, the piezoelectric crystal, when applying an external stress. They are characterized by their sensitivity which is the ratio of the piezoelectric actuator movement to the piezoelectric actuator voltage. When under stress, the piezoelectric crystal structure deforms. Some atoms are either getting closer or pushed apart upsetting the balance of positive and negative charges: net electrical charges appear on opposite outer faces of the crystal. The opposite of this effect, called reverse piezoelectric effect, is used in AFM scanners. A voltage is put across the crystal. The atoms have to move to rebalance the structure causing deformation of the piezoelectric crystal.

3.1.4 The components of the detection method

Two main detection methods exist: the optical one and the electric one. The AFM used (NanoWizard Ultraspeed, JPK) is based on an optical detection method: the light beam deflection. A light beam is reflected off the back of the cantilever onto a segmented photodiode. The reflected laser spot must be in the center of the photodetector to maximize the sensitivity for imaging and force control. This is done by tilting a mirror for a coarse

adjustment of laser path and then by using positioning screws for a fine adjustment (see Figure 3.4). The photodetector is equally segmented in four quadrants generating a voltage proportional to the amount of incident light [35]. When scanning a surface, the deflection, due to topographic changes, is expressed as the difference in voltage between the top and bottom halves of the photodetector: $Deflection = V_{\text{top}} - V_{\text{bottom}} = (V_{\text{A}} + V_{\text{B}}) - (V_{\text{C}} + V_{\text{D}})$. Deflection in volts can be transform to nanometers knowing the sensitivity of the cantilever (see 4.2), assuming linearity only for small deflections.

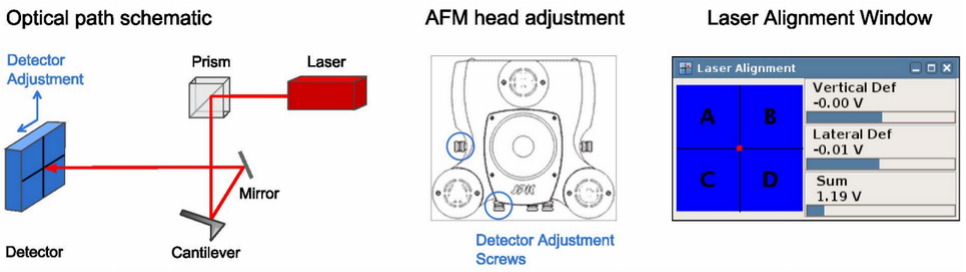

Figure 3.4: (A) Schematic representation of the detection method
(B) AFM head with adjustment screws
(C) Laser Alignment window representing the four segments of the detector

3.2 Basic imaging modes

When scanning, the AFM tip covers a line in the x direction and then moves in the y direction to cover the next x line. Changes in topography of the sample induce bending of the cantilever. A signal is created and fed back to a control system to maintain the deflection to a certain constant level, the setpoint. This is done by adjusting the Z-piezo height to keep the imaging force constant. The AFM image is a plot of the z correction distance against the x and y directions: a three dimensional perspective of the surface is obtained.

3.2.1 The Lennard-Jones potential

The Lennard-Jones potential is used to represent the force between two non-bonding atoms or molecules based on their distance of separation and is expressed as below:

$$V(r) = 4\epsilon[(\frac{\sigma}{r})^{12} - (\frac{\sigma}{r})^{6}] \tag{3.1}$$

With:

- V the intermolecular potential between the two atoms or molecules.
- σ the distance at which the intermolecular potential between the two particles is zero i.e. representing how close two non-bonding particles can get. It is called the Van der Waals radius.
- ϵ the well depth representing how strongly the two particles attract each other.
- r is the distance of separation between the center of the two particles.

Figure 3.5 describes the Lennard-Jones potential. When the two particles are at an infinite distance apart, the possibility that they interact is minimal and their bonding potential

energy is considered equal to zero. As the distance decreases, the probability of interaction increases. At some point, the particles are reaching a distance of separation where they become bound. The bonding potential energy starts decreasing from zero to a negative value. This is indicated as the attractive force on figure 3.5. Attraction between the two particles occurs until reaching equilibrium, which is specified by the separation distance at which the minimum potential energy is reached. At this point, the pair of particles is most stable and will remain in that orientation until an external force is exerted upon it. If the separation distance keeps to decrease, repulsion occurs. The two particles are so close that their electrons are forced to occupy each other's orbital. Each particle tries to retain their respective orbital causing repulsive forces. In this region, the bonding potential energy increases rapidly as the distance of separation decreases (as indicates as the repulsive force on figure 3.5) [36].

The three most common AFM imaging modes operate under these different force regimes as described below [37] :

- The non contact mode is in the attractive force regime: as probe and surface approach, Van der Waals interactions pull the probe toward the surface,
- The contact mode is in the repulsive force regime: when contact is made, interactions become repulsive and pressing the probe against the surface causes an upward deflection of the cantilever,
- The intermittent contact or tapping mode can be used in the attractive or repulsive regime. The probe is oscillating, with alternations between in and out of contact with the surface.

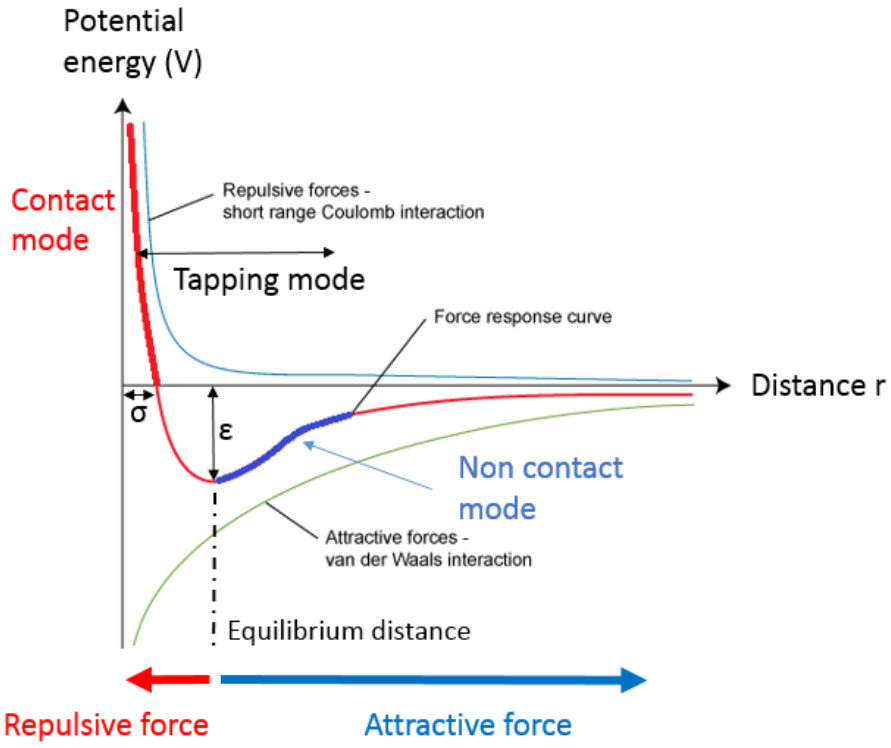

Figure 3.5: Diagram of the forces regimes under which AFM imaging modes operate

3.2.2 Contact mode

Contact mode or DC mode is the simplest imaging mode during which the AFM cantilever remains in contact with the sample by maintaining a constant deflection over it i.e. a constant force. This is done using a feedback control (see below 3.3) on the measure of deflection. Two variations exist: constant force or variable force. The applied force during imaging is adjusted by changing the amount of deflection of the cantilever onto the sample. Too high forces can however damage the sample or result in a contaminated tip. Lateral forces, which can result from frictional forces, can also be a problem and damage the sample or the tip.

3.2.3 Intermittent contact mode

In tapping mode or AC mode, cantilever oscillates at a value close to its resonance frequency while scanning the sample. The tip spends less time in contact with the surface reducing therefore the lateral forces and possible artifacts due to adhesion. Surface topography is obtained using the feedback control to vary the Z-piezo height and maintain a constant amplitude. This mode can be used in dry or in liquid. The AFM tip is less time on the sample surface, increasing its lifetime. Care should be taken to stay either within the attractive or repulsive regime, the repulsive regime being the most used.

3.2.4 Non-contact mode

In non-contact mode, the AFM tip oscillates above the surface at smaller amplitude than for the tapping mode. The contact period with the surface is very small or zero. Van der Waals attractive forces between sample and tip produce a dampening effect on the cantilever according to the topography of the surface. When encountering protruding features on the surface sample, the oscillating amplitude of the cantilever decreases. The shift between driving and oscillating frequencies or the oscillating amplitude itself are used in the feedback loop to adjust the Z-piezo height and ensure to maintain the tip out of contact.

3.3 Feedback loop control

When performing AFM imaging, the signal is fed-back to a control system to adjust the Z-piezo distance from the sample's surface in order to maintain the deflection at the setpoint level. On-off control is the most basic feedback loop control operation but it is unable to reach the setpoint level: signal would oscillate and results would not be accurate enough for AFM imaging. Mathematical terms are thus used to have a better control on the signal: the proportional (P), the integral (I) and the derivative (D). Below the PID control diagram:

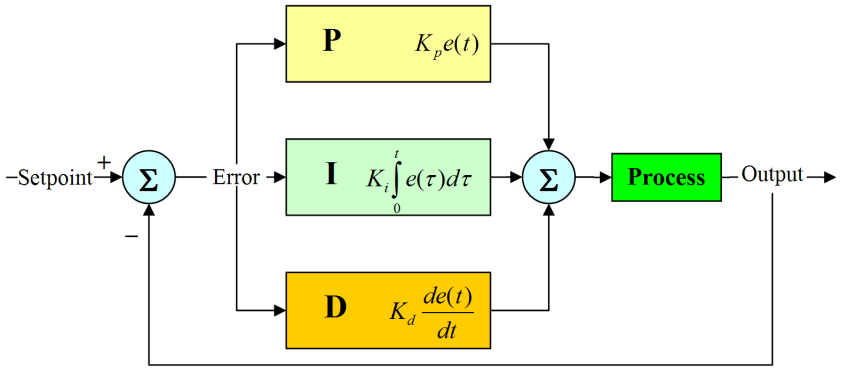

Figure 3.6: PID control diagram with the three characteristic parameters: the proportional gain (K_p), the integral gain (K_i) and the derivative gain (K_d)

The proportional term is the immediate response to the error. It amplifies the error between the setpoint and the measured value by defining a proportional band. This band is a percentage of the total span of the controller. Proportional gain and band are related. If the proportional band is 25%, the gain is 4. Higher gain leads to smaller band. This operation results in an offset of the signal from the actual setpoint. However, using only the proportional term, the setpoint can not be reached: a residual steady-state error stays. The integral term is used to remove small errors. It integrates the deviation from the setpoint over a period of time in order to remove the offset or steady-state error. Time response of the piezoelectric scanner defines this time period. Too small time will generate oscillations and the response will become unstable. Even a small error term will cause the integral component to increase slowly. However, it can also cause the value to overshoot the setpoint limit. The response of the controller after applying first a proportional term only and then a proportional and an integral term is shown in Figure 3.7.
The derivative term is applied to reduce the tendency of the controller to erratic behaviour. It causes the output to decrease, if the process variable is increasing rapidly. If the sensor feedback signal is noisy or if the control loop rate is too slow, it can however lead to instability of the control system. For this reason, the derivative term is thus most often set to zero.

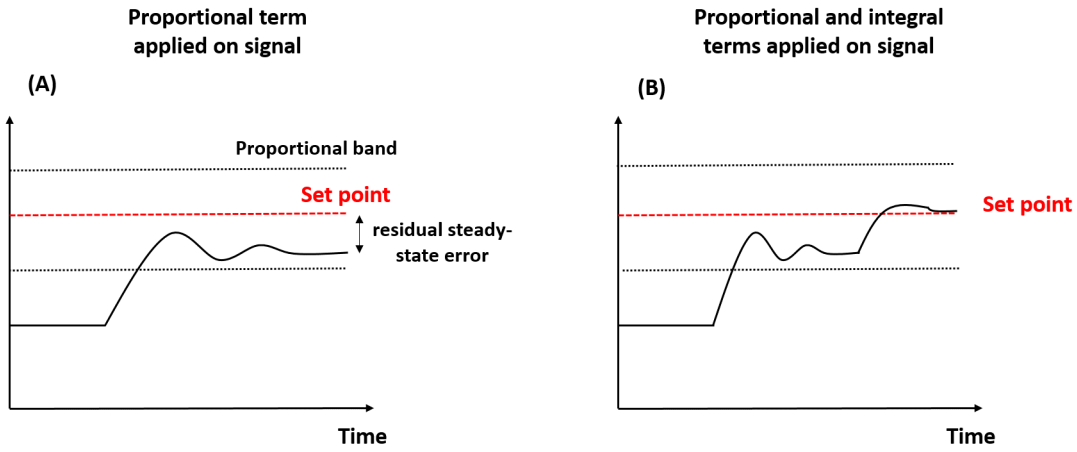

Figure 3.7: In (A), proportional term is applied to the control signal
In (B), proportional and integral terms are applied to the control signal

Chapter 4

Materials and Methods

4.1 Collagen sample preparation

Collagen samples were obtained from tail-tendon of two wild mice of 6 months old. Initially, fiber bundles were harvested from a tendon section using a scalpel and tweezers. Then the fiber bundles were spread out onto a microscope glass slide surface using the tweezers. This was done by hydrating the fibers and separating them to reveal individual collagen fibrils. After drying, the fibrils adhere to the glass slide surface and remain adhered even after rehydration.

For the nanoindentation experiments, three samples were tested. For the nanotensile experiments, four fibrils were tested under different experimental conditions (see part 4.3.4).

4.2 Calibration for atomic force microscopy cantilever-based experiments

Calibration was performed prior to each experiment to determine the sensitivity as well as the spring constant of the cantilever. The spring constant is calculated once in air. However, the sensitivity must be re-determined when experiments are performed in liquid. The sensitivity depends on the displacement of the laser spot on the photodetector. When the cantilever is immersed in liquid the laser enters a medium with different refractive index. Due to the difference in refractive index the laser spot will move to a different extent in liquid than in air. For this reason the sensitivity was calculated for all different solutions used.

The sensitivity was calculated by performing a force map of 2*2 on the stiff glass surface. In total, 4 deflection (Volts) versus displacement (Z piezo displacement in nanometers) were obtained per medium. The inverse slope of the deflection-displacement curve is the sensitivity value in nm/Volts (see Figure 4.1). For each medium, the mean of the inverse slope of the 4 curves resulting form the retract signal was set at the cantilever sensitivity. This parameter is an important scaling factor that changes the volts deflection into nanometers which is then used in Hooke's law to determine the applied force.

The spring constant is calculated using the thermal noise method ([38]). The method is

based on the simple harmonic oscillator equations [39]:

$$A^2(f) = \eta^2 + {A_{DC}}^2 * \frac{{f_0}^4}{({f^2 - {f_0}^2})^2 + \frac{f^2 * {f_0}^2}{Q^2}} \tag{4.1}$$

with A_{DC} the DC amplitude, η the white noise background, f_0 the resonance frequency and Q the quality factor (width of resonance).

When oscillating the cantilever away from the surface, a plot of the fluctuations as a function of frequency can be acquired. This is the thermal noise spectrum. The cantilever is susceptible to thermal deflections resulting in small forces impulses visible on the spectrum peaks. The amplitude depends only on the spring constant of the cantilever at a given temperature. The AFM system measures the size of the fluctuations. The measurements are analyzed by looking at the frequency dependance of the fluctuations. Analysis of the data are, thereby, more focused on the resonance peak and noise sources are excluded. After fitting using a Lorentz function at the resonance peak, the area under the curve is used as a measure of the energy in the resonance. The equipartition theory says that the energy in any free mode of the system has to be equal to the thermal energy due to the absolute temperature of the system ([39]), i.e. that:

$$\frac{1}{2} * k * q^2 = \frac{1}{2} * k_b * T \tag{4.2}$$

With k_b the Boltzmann constant, k the spring constant and q the average value of the vertical deflection of the cantilever. The value of q^2 is the measured value from the Lorentz fit to the frequency spectrum. The spring constant can then be calculated. Additional correction factors are added to obtain a more accurate value from the fit, the movement of the cantilever being not completely harmonic.

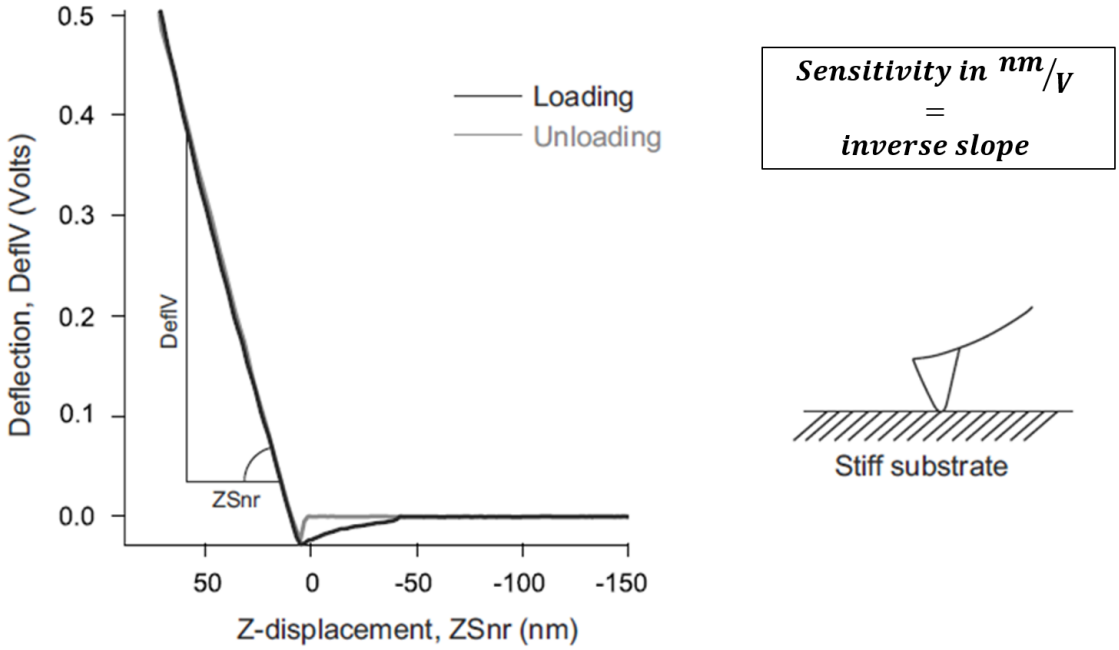

Figure 4.1: Typical deflection (Volts) versus displacement (nanometers) curve obtained on a stiff substrate (i.e. glass slide)
DeflV: Deflection in volts - ZSnr: vertical displacement of the piezocrystal
Adapted from O. Andriotis (2013) [5] with permission.

4.3 Experimental protocols

4.3.1 Choice of the cantilevers

Cantilever-based nanoidentation was conducted using the PNPDB cantilevers (A) with tips from NanoWorld. The nominal spring constant of the cantilever is 0.48 N/m. A cantilever with spring constant similar to the apparent spring constant of the fibrils is required to optimize sensitivity and signal to noise ratio [23]. Stiffer cantilevers provide a higher signal to noise ratio. However, when in combination with small indentation depth, accuracy of the measurements is decreasing due to the small cantilever deflection. Prior to nanotensile tests, fibrils were imaged using the same cantilever. The nanotensile experiments were done with a stiff and tipless cantilever, all-in-one from Budget Sensors (AIO, Budget Sensors). The nominal spring constant of the cantilever is 40 N/m. This choice was made to prevent from too large deflection of the cantilever when moving the Z-piezo away and thus maximize the pulling of the fibril.

4.3.2 Choice of the solution of increasing polyethylene glycol concentration

Initially, six solutions were prepared: a phosphate buffered saline solution (PBS) and five solutions of polyethylene glycol (PEG) in PBS of molarity 0.1M, 0.5M, 1M, 2.6M and 3.5M.

PBS of concentration 0.01M was used. Chosen PEG (H(OCH2CH2)nOH with n=4.2) has an average molecular weight of $200 \pm 10 g \cdot mol^{-1}$ and a density of $1.1239 g \cdot mol^{-1}$ at $20°C$. Seven different set of data, including the imaging performed in air, were obtained from the nanoindentation experiments. After the analysis of the results as described below in 5, it was decided to have three other solutions to supplement the results: PEG in PBS of 1.5M, 2M and 2.3M (i.e. of PEG concentration of 2mol/L, 3mol/L and 4mol/L). Both nanoindentation and nanotensile experiments were carried on in these nine solutions.

4.3.3 Protocol and process for nanoindentation of an individual collagen fibril

Contact mode imaging was used in air-dried samples and the quantitative imaging mode (QI^{TM}) was used for imaging in liquid. The contact mode in liquid results in artifacts from the lateral movement of the cantilever over the sample.

QI mode is similar to a force volume map, during which the cantilever performs force curves over a region of interest. In contrast to force volume maps, the QI mode is a faster version and image resolution can be up to 512x512 pixels. At each pixel a force-displacement curve of the image is completed similar to the one presented before in Figure 4.1. After performing each curve, the tip is moved to the next position as shown on Figure 4.2. In QI mode the tip is not scanning in the XY while in contact with sample but only approaches on the surface of the sample, the lateral forces are diminished. In this way, QI mode prevents from undesired damages of the sample and artifacts. Additionally the vertical force is controlled to a predefined value and hence force measurements are possible. It is also possible to scan in solutions with a quite high resolution. A dynamic baseline adjustment can be done while imaging in fluids to consider the hydrodynamic effect. All information about the local tip-sample interaction are obtained through the force-displacement curves. The height data can be extracted, with the sensor height at the triggered point as the standard value. The indentation modulus can also be obtained from the loading or the unloading part of the force-displacement curve.

While imaging in air and for each sample, a region of interest of 20 μm x 20 μm was defined with at least 4 native collagen fibrils recognizable by their periodic D-banding. The 4 native collagen fibrils were then imaged individually in air in 2.5 μm x 2.5 μm scale. Subsequently, the same collagen fibrils were then imaged when hydrated in PBS and in increasing concentration of PEG. QI mode parameters were defined as below:

- Set point= 2nN,
- Z-length= 90nm,
- Constant speed imaging,
- Extend speed= $18 \mu m \cdot s^{-1}$,
- Resolution in pixels of 256x256.

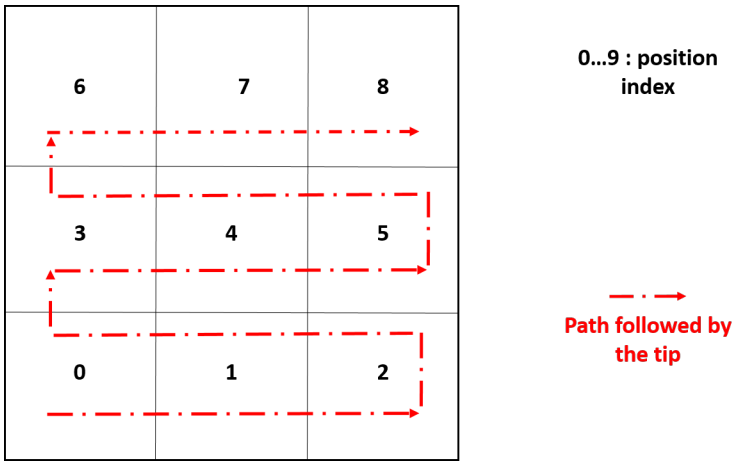

Figure 4.2: Schematic illustration of the path followed by a tip for an image resolution of 3*3

4.3.4 Protocol and process for nanotensile testing of an individual collagen fibril

Gluing of a collagen fibril

Before being able to perform nanotensile experiments, individual collagen fibril has to be carefully glued to the substrate at one end and to the tipless cantilever at the other end. After finding a good region of interest, i.e. a region where at least 4 native collagen fibrils are recognizable and well separated, imaging of the fibrils in each medium was performed. Subsequently, gluing and scrapping processes were done in three main steps:

- First step - the gluing of an individual collagen fibril at each end: A 90 min UHU epoxy resin was used. Epoxy resin of lowest working time are too soft when drying on the sample. The two components of the epoxy have to be well mixed to prevent from microscale soft droplets and pre-cured for about 40 min (until the epoxy starts to be viscous). A droplet is then placed on the glass slide away from the fibril since it could otherwise submerge the sample (see (1) on Figure 4.3). A thin tool as an eyelash mounted on a tooth pick has to be used. A micro-droplet is then taken from the droplet using a tipless cantilever and applied at each end of the fibril (see (2)). The tipless cantilever is placed over the droplet and approach is done until reaching the droplet. At this moment, some of the epoxy is sticking to the cantilever and the Z-piezo has to be retracted away from the sample. By approaching over the two ends of the collagen fibril, epoxy is attached (see (3)). Waiting time of about 10 hours is then necessary to obtain a fully cured epoxy.

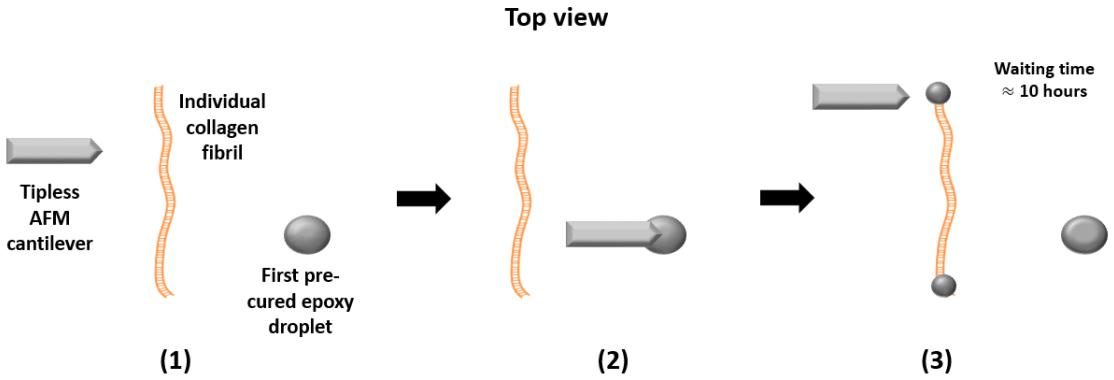

Figure 4.3: Schematic illustration of the first gluing of an individual collagen fibril

- Second step - the scrapping process: One of the fibril's ends will be pulled during the experiments. This fibril's end has to be freed from the surface and glued to the cantilever. Done on dry samples, small indents are made into the epoxy from the rear side and repeated further along the edge of the glue using a stiff cantilever with a tip (see (4) on Figure 4.4). When two thirds of the epoxy is detached, the rest is likely to detach in one go (see (5)). If the pre-cured period was not long enough, the epoxy will stay glued to the surface.

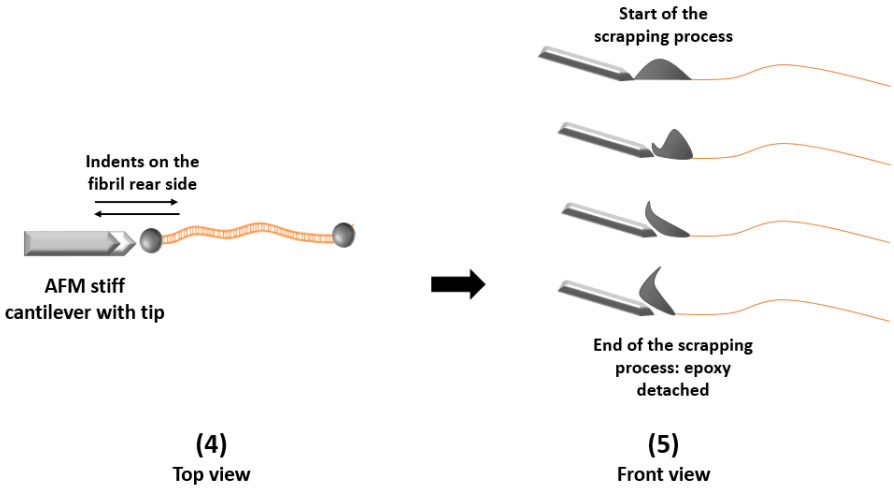

Figure 4.4: Schematic illustration of the scrapping process of an individual collagen fibril's end

- Third step - the gluing of the freed end of the fibril to the tipless cantilever: A second epoxy (9O min UHU as before) is prepared but with a lower waiting time of about 20 min. As done before, it is then applied on the glass slide and taken with a tipless cantilever (see (6) on Figure 4.5). The micro-droplet taken has to only be glued to the freed end of the fibril. To obtain a smaller droplet of epoxy, the cantilever was brought in contact with the substrate for several times. At each contact some epoxy was left at the glass and a smaller portion on the cantilever (see (7)). It will prevent gluing the end of the fibril, the glass slide and the cantilever together. Finally, the freed end of the fibril is glued to the cantilever (see (8)). This part is the most

delicate, and approach of the cantilever has to be done slowly. Waiting time of about 10 hours is again necessary to obtain a fully cured epoxy.

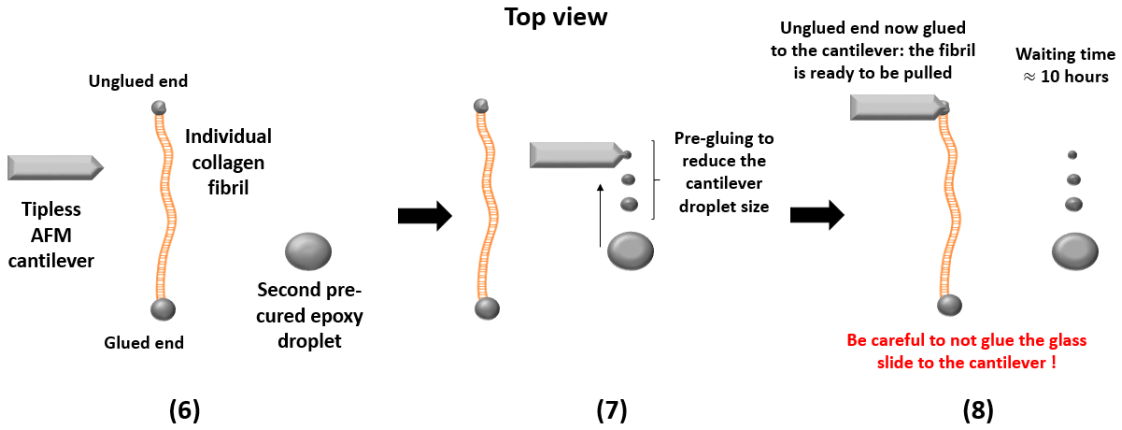

Figure 4.5: Schematic illustration of the second gluing of an individual collagen fibril

Finding the zero strain length of a collagen fibril

The collagen fibril has to be set in its resting position or zero strain length, i.e. when extended but not pulled. PBS is added since moving the cantilever in air may cause breaking of the fibril. The cantilever position has to be adjusted in order to truly pull the fibril perpendicular to the substrate.

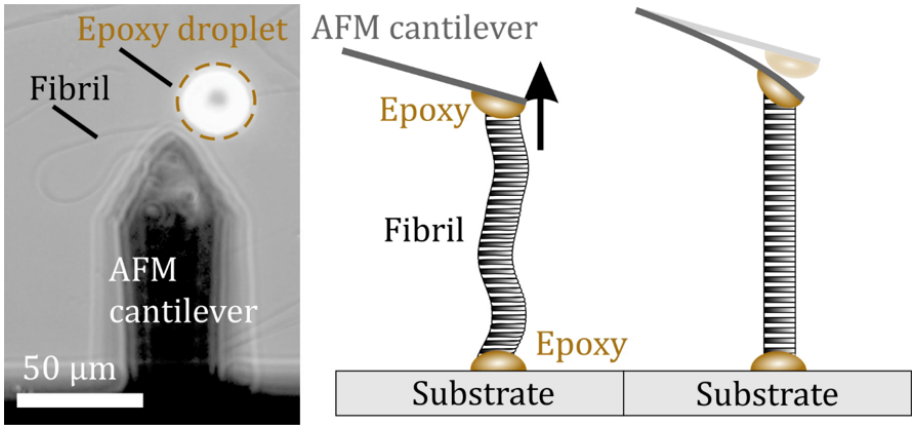

Figure 4.6: Schematic illustration of the gluing process

This is done following the steps below:

- The cantilever (glued to one of the fibril's end) is moved of few μm away from the surface and brought closer to the second fibril's end. The cantilever is not deflected since the fibril is not pulled. On the laser alignment window, the laser point is at the zero position, i.e. at the center of the 4 segments.
- The cantilever is then slowly moved away (1μm per 1μm) until the cantilever starts to deflect The laser point is not anymore at the zero position. However, the zero strain length of the fibril may not be reached yet. The fibril is not necessary perpendicular to the substrate but may be tilted.

- In order to reach the zero strain length, the cantilever is delicately moved in small circles around its position until finding at which location the deflection of the cantilever is the lowest. On the laser window, the laser point is at this moment at the zero position or as close as possible from it.
- The cantilever is slowly further moved away from the surface (few μm) to have the fibril under loading. Zero strain length of the fibril is found by subtracting the Z-piezo height of the loading state to the total distance from the surface. The Z-piezo height of the loading state is obtained on the deflection-displacement curve: when the cantilever starts to deflect, i.e. when the slope is increasing, the fibril is no longer in its zero strain length (see Figure 4.13).

Pulling of a collagen fibril

Nanotensile experiments were displacement controlled by controlling the displacement of the Z-piezo. Displacement of the Z-piezo is controlled via the force ramp designer. It defines the movement of the Z-piezo as well as the number of recordings of loading and unloading curves of the vertical deflection against the Z-displacement.
First the Z-piezo is fully retracted (since it is away from the surface) and the fibril is loaded, then the Z-piezo is extended, which results in unloading the fibril and then the Z-piezo is again retracted which results in a loading.

Parameters for the force ramp designer were defined as below:

- An "'Extend"' step,
- An optional waiting step at one specific height,
- An "'Retract"' step.

For the "'Extend"' and the "'Retract"' steps, the length of the recording points were chosen to 5 μm. Also, the speed has to be defined. This parameter can be variable to analyze the influence of the strain rate. A waiting step can also be added to test the effect of a resting time on the cyclic loading.
For the 4 fibrils tested, different experimental conditions were defined:

- For the first two fibrils, 6 loading cycles were implemented in each solution. The speed was fixed to 0.5 μm and and no resting time was applied.

- For the third fibril, resting time was tested in each of the solutions. The speed was fixed to 0.5 μm and an increasing resting time was set i.e. 0 sec, 10 sec, 30 sec and 60 sec. 6 loading cycles were implemented in each solution at each resting time.

- For the fourth fibril, strain rate was tested in PBS and solutions of 1M, 2.6M and 3.5M PEG in PBS. Resting time was set to 10 sec. Increasing strain rate were equal to 0.4 %/sec, 1 %/sec, 5 %/sec, 10 %/sec, 20 %/sec, 40 %/sec and 80 %/sec.

4.4 Data analysis

4.4.1 Nanoindentation of collagen fibrils at various osmotic pressures

Determination of the diameter of a collagen fibril

To determine the diameter of one individual collagen fibril, a Matlab script was used. Processing of data was done as below (as shown in Figure 4.7):

- First, the erratic data from imaging artifacts were corrected by polynomial fitting to the height image using the JPK data processing software.

- Conversion values were applied to the raw data of the JPK and JPK QI image of the height to obtain data in nanometers. These data correspond to the addition of the height of both the fibril and the glass (on Figure 4.7 (1))

- Leveling was applied to remove tilt (2).

- A region of interest selected so that crest of the fibril is fully included in that region. The region of interested was selected by cropping the image from 256x256 resolution to 256x156 i.e. removing 50 lines from the top and bottom of the image (3).

- A mean value of the glass height was then calculated by covering each line in both directions (from the left and from the right) until reaching 10% of the maximum value of the line (i.e. the crest of the fibril). At this point, it is necessary to move back 20 pixel in each direction to only consider the glass. The remaining data from the right and left sides of each line constitutes the glass only. The mean of these values was defined as the glass height and subtracted from the data (4).

- Each cross section line includes one maximum (the crest of the fibril), and there are 156 lines i.e. 156 height data for a given fibril. From these 156 data the average diameter of the fibril was calculated (5).

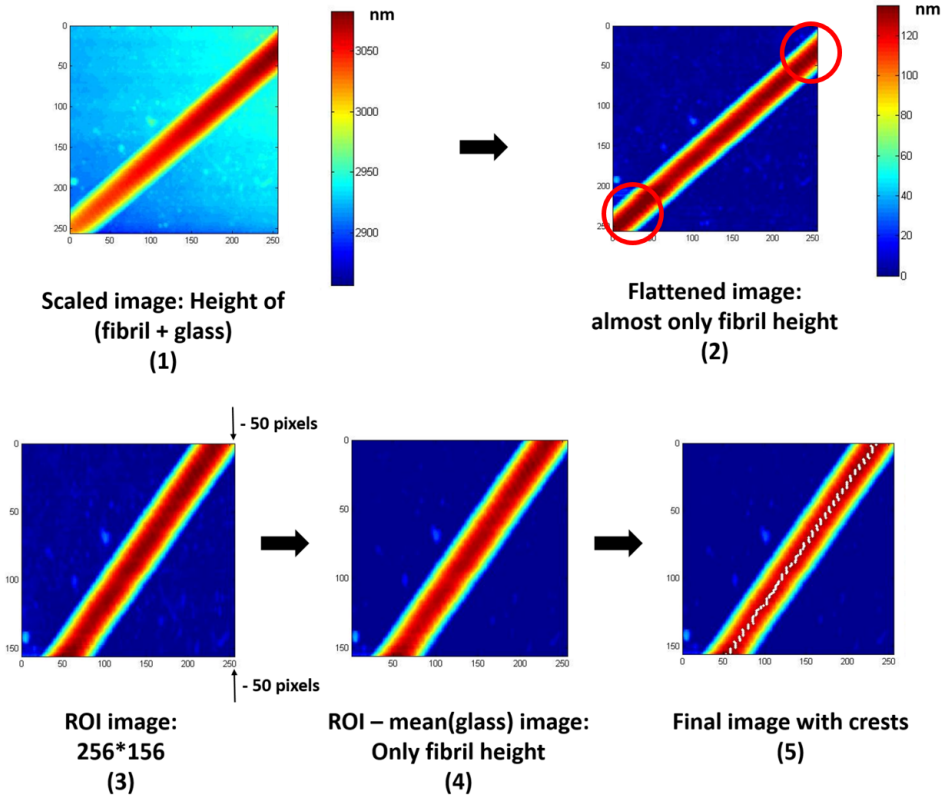

Figure 4.7: Atomic force microscopy height topography images for a fibril through the height analysis procedure.

Swelling and shrinking at the collagen fibril level

The tested collagen fibrils were first imaged in air dried condition. When PBS is added, water is absorbed by the collagen fibril. Separation distance between the collagen molecules increases and the collagen fibril swells. The swelling can be determined knowing the diameter of the fibril in both air and PBS by the equation:

$$Swelling(\%) = \frac{height_{PBS}}{height_{air}} * 100 - 100 \tag{4.3}$$

With $height_{PBS}$ and $height_{air}$ the average values of the diameter (or height) of the fibril in air and in PBS calculated as explained previously 4.4.1.

One hypothesis of the thesis is relative to the influence of the osmotic pressure generated by proteoglycans to reduce the diameter of the fibril. The fibril is initially hydrated, when in PBS. When proteoglycans are added in the ECM, i.e. when PEG is included in the PBS, the collagen fibril would dehydrate and shrink. In the experiments done, the fibril is initially hydrated in PBS. A solution of defined concentration in PEG is then replacing the PBS. The shrinking from PBS to the PEG in PBS solution is defined as:

$$Shrinking(\%) = 100 - \frac{height_{PEG}}{height_{PBS}} * 100 \tag{4.4}$$

The schematic illustration 6.1 represent the swelling and the shrinking at the collagen fibril level as defined in the hypothesis.

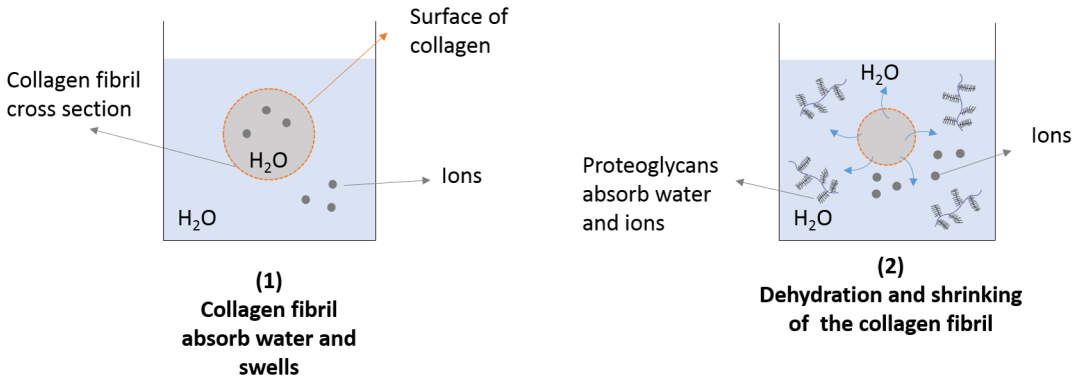

Figure 4.8: Hypothesis of swelling and shrinking of an individual collagen fibril under osmotic pressure.

Determination of the projected area of contact between the indenter and the sample

The projected area of contact between the indenter and the sample is needed in order to determine the indentation modulus. The tip of the cantilever used is defined as below:

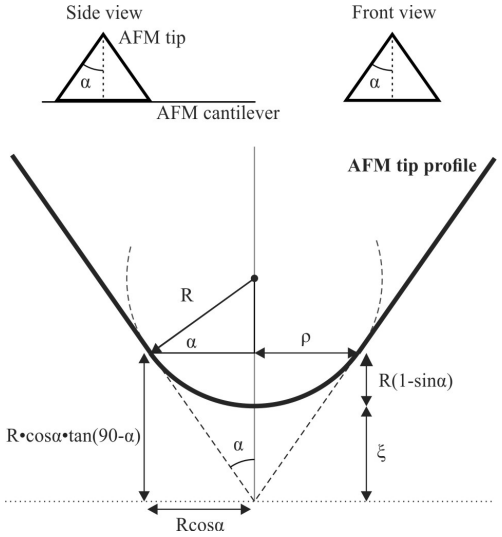

Figure 4.9: Geometrical schematic of the PNPDB tip

The projected area of contact is estimated by assuming a pyramidal geometry with a round tip of radius R and half opening angle α ([40]).The area of the tip is then :

$$A_c(h) = 4(h + \xi)^2 * (\tan \alpha)^2 \tag{4.5}$$

with h the indentation depth, ξ the correction distance and α the half opening angle. The correction factor ξ is determined by:

$$\xi(R, \alpha) = R(\sin \alpha + \cos \alpha * \tan (90 - \alpha) - 1) \tag{4.6}$$

The equation given for the projected area of contact is valid for indentation depth $h > R(1 - \sin a)$. In this study, the tips used have a radius of 10 nm and a half opening angle α of 35 deg.

Determination of the indentation modulus of a collagen fibril

AFM cantilever-based nanoindentation allows to access data concerning the height and the stiffness of collagen samples. As explained previously, the AFM tip indents the surface at a predefined loading-unloading rate to reach the maximum deflection of the cantilever. The tip is then retracted away from the surface until the deflection of the cantilever is again zero (i.e. no contact with the sample). The total displacement of the Z-piezo is equal to the sum of the deflection of the cantilever and the indentation depth of the tip. According to Bueckle's law ([41]) and the results from a recent statistical analysis ([7]), the maximum indentation depth should be inferior or equal to 15 % of the sample thickness to avoid substrate effects. From the force-displacement curves of the vertical deflection in function of the Z-piezo displacement recorded, the force is calculated by Hooke's law:

$$Force(N) = k(N/m) * Deflection(m) \tag{4.7}$$

with k the spring constant of the cantilever. The projected contact area between the tip and the sample depends on the size of the indenter. AFM tips are relevant to use to determine nanomechanical characteristics of collagen fibril: they have a low projected contact area function and detect several nanometers of the cantilever deflection (see Figure 4.10). Height data are directly accessible after applying scaling factors on the raw values. Post analysis is required to access elastic modulus values as suggested by Oliver and Pharr [42] .

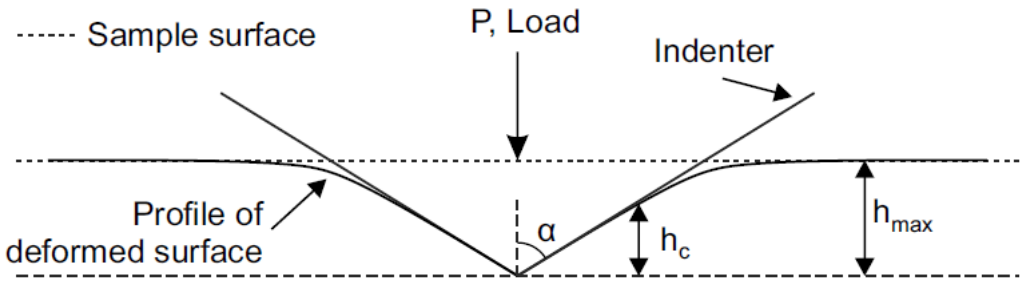

Figure 4.10: AFM tip indentation on a flat surface. h_{max}: Maximum indentation depth; h_c: Contact indentation depth; α: Half opening angle.
Adapted from O. Andriotis (2013) [5] with permission

Oliver and Pharr method:

Unloading curves of nanoindentation experiments are analyzed to obtain values of elastic modulus avoiding plastic contributions ([42] and [43]). Unloading curves are characterized by a power law function:

$$F = m\,(h - h_0)^n \tag{4.8}$$

where h_0 is the permanent indentation depth after unloading, m (N/m^n) and n (dimensionless) are fitting parameters along with h_0. The contact stiffness $S_c = dF/dh$, necessary for the elastic modulus calculation, is defined as the slope of the upper 75% of the unloading curve.
Calculation of the contact stiffness requires several steps:

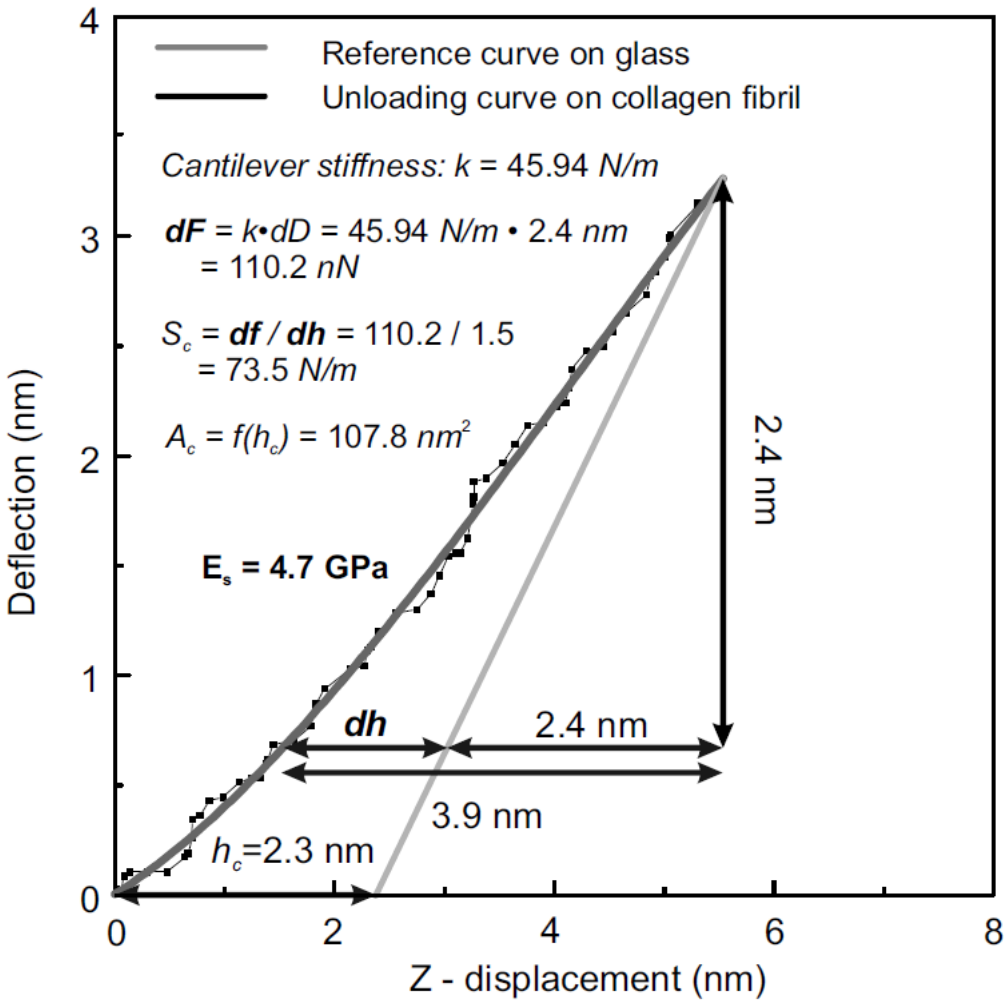

Figure 4.11: Deflection versus z-displacement of AFM nanoindentation unloading curve and required parameters for the elastic modulus calculation.
Adapted from O. Andriotis (2013) [5] with permission

As it is shown in the figure 4.11 the maximal values on the x-axis Z_{max} and on the y-axis D_{max} as the slopes of the linear part of the unloading curve $Zslope_{unloading}$ and of the glass curve $Zslope_{glass}$ are directly determined. This allow to calculate the contact stiffness using:

$$dh = D_{max} * (\frac{1}{Zslope_{unloading}} - \frac{1}{Zslope_{glass}}) \tag{4.9}$$

and

$$dF = k * D_{max} \tag{4.10}$$

Now that the contact stiffness is obtained, the projected area of contact has to be calculated (see equation (4.5) for the detailed calculations) in order to calculated the elastic modulus. The projected area of contact is a function of the contact depth h_c:

$$h_c = h_{max} - \varepsilon \frac{F_{max}}{S} \tag{4.11}$$

where the value of ε is a constant that depends on the indenter geometry (see equation (4.6)) and $h_{max} = Z_{max} - D_{max}$.

The reduced elastic modulus formula correspond to the deformations of both bodies when being in contact:

$$E_r = \beta \frac{\sqrt{\pi}}{2} \frac{S_c}{\sqrt{A_c}} \tag{4.12}$$

where β is a dimensionless parameter that varies with indenter shape ($1.0226 < \beta < 1.085$), here β is taken equal to 1.
The reduced elastic modulus of the two elastic bodies in contact can also be expressed as:

$$\frac{1}{E_r} = \frac{1 - \nu_s^2}{E_s} + \frac{1 - \nu_i^2}{E_i} \tag{4.13}$$

where ν_s and ν_i the Poisson's ratio of the sample and indenter respectively and E_s and E_i the indentation and elastic modulus of the sample and indenter respectively. Poisson's ratio is assumed to be 0.5 for collagen fibrils [23], [44]. The elastic modulus of the silicon AFM tip is much larger than the collagen samples studied ([45]), thus $E_i \ll E_s$ and the equation (4.13) is simplified by neglected the indenter part. By substitution in the equation (4.12), the elastic modulus of the sample is finally:

$$E_s = \beta \frac{\sqrt{\pi}}{2} \left(1 - \nu_s^2\right) \frac{S_c}{\sqrt{A_c}} \tag{4.14}$$

For a faster and easier repeatability of the data processing, post-processing can be done in a Matlab script following the calculations explained previously. The Oliver-Pharr method is not supported in the JPK data processing software, but analysis can manually be done using the hertzian theory.

Hertzian theory:

This theory assumes pure elastic deformation between two bodies and defines the indentation modulus as below:

$$E = \frac{3F_{max}}{4\sqrt{R_{eff}}} h_{max}^{-3/2} \tag{4.15}$$

With F_{max} the maximum applied load, h_{max} the maximum indentation depth and R_{eff} the effective radius depending on the assumptions made for the geometry of the two bodies in contact.
This theory can be directly applied in the JPK software entering parameters relative to the tip and the sample analyzed (Poisson's ratio). Each curve at each location of the QI data are post-processing and elastic modulus on the locations of the maximum height of the fibril can be obtained. It gives an estimation of the elastic modulus of the fibril analyzed but is not as precise as the Oliver and Pharr method since plastic deformation is not removed. However, the hertzian theory was chosen to analyze the data because of a technical reason. At the moment, the data from the QI files could not be extracted and analyze separately since too many files are included in the QI archive.

4.4.2 Nanotensile testing of collagen fibrils at various osmotic pressures

Viscoelasticity of an individual collagen fibril

Viscoelastic materials exhibit both elastic and viscous characteristics. The material is able to recover to its initial shape during unloading but following a different path compared to the loading one, a phenomenon which is also known as hysteresis. The Kelvin model is the simplest model describing this phenomenon considering a dashpot acting in parallel of an elastic spring [19] . The mechanical behavior is then time dependent and can be expressed via the equation [46]:

$$\sigma = E\epsilon + \eta\dot{\epsilon} \tag{4.16}$$

The two curves below illustrate the differences between elastic, plastic and viscoelastic deformations (Figure 4.12). On a typical stress-strain curve, the yield strength refers to the limit between elastic and plastic regions.

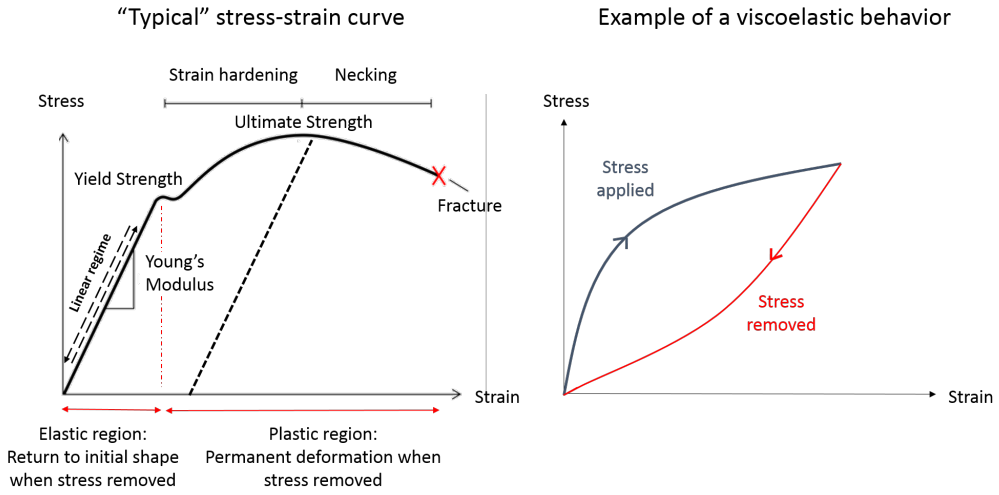

Figure 4.12: Comparison of stress-strain curves to illustrate viscoelastic behavior

Determination of the longitudinal stiffness on a collagen fibril

Nanotensile tests return curves of the loading and unloading. After applying the required conversion values to the raw data, the vertical deflection and the Z-piezo height are obtained. In figure 4.13, the vertical deflection, i.e. the force, is not reaching the same value for the loading and unloading curves due to the limitation of the AFM model. The fibril is, indeed, initially pulled. The cycles are then unloading-loading and not loading-unloading.

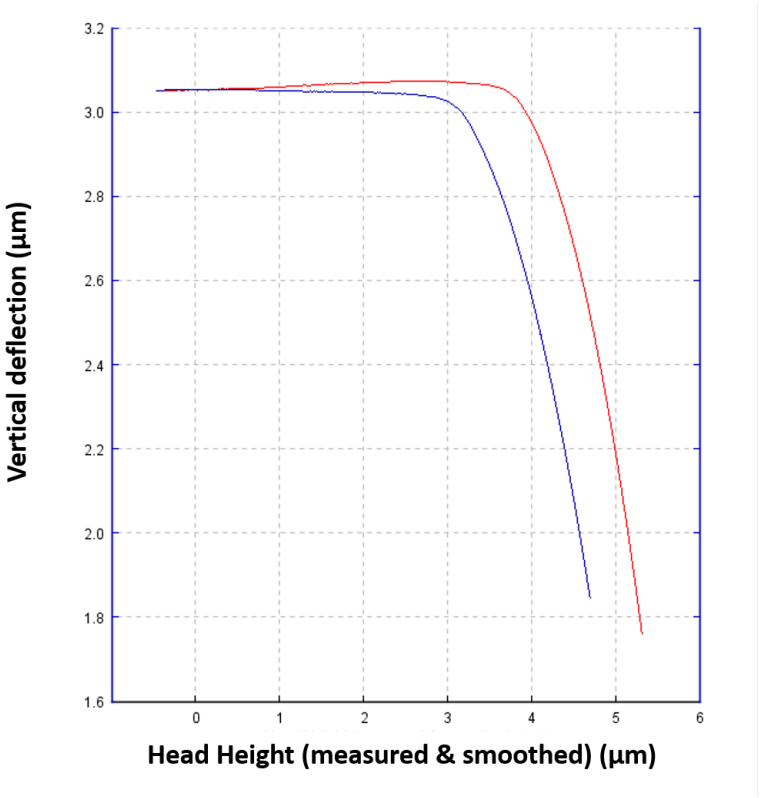

Figure 4.13: Vertical deflection in function of the Z-piezo height as obtained in the PJK AFM software
in red: unloading curve and in blue: loading curve

Force displacement curves can now almost directly be plotted. The force is obtained through Hooke's law (see equation (4.7)) applied to the vertical deflection data. The displacement ΔL corresponds to the differences between each point of the Z-piezo height recorded.
Stress-strain data are deduced from these data as well as from the fibril's diameter and zero strain length:

$$\sigma = \frac{F}{A} = \frac{F}{\pi * (D/2)^2} \tag{4.17}$$

and

$$\epsilon = \frac{\Delta L}{L_0} = \frac{L_i - L_0}{L_0} \tag{4.18}$$

With L_0 the zero strain fibril length, L_i the fibril length at one precise point of the pulling process and D the fibril diameter. Longitudinal stiffness at each strain is given by the slope of the strain-stress curve.
A Matlab script was implemented to perform these calculations and find the location of the contact point on each curve; point at which the fibril starts to be pulled. Before this point the fibril is at its zero strain length. The elastic modulus $E = \frac{d\sigma}{d\epsilon}$ is, then, no longer a constant but a function of strain $E = E(\epsilon)$. In the same way, the stiffness is also a function of strain $S = \frac{dF}{dL} = S(L) = S(\epsilon)$.

Chapter 5

Results

5.1 Nanoindentation of collagen fibrils at various osmotic pressures

5.1.1 Swelling of collagen fibrils in PBS at physiological pH

From imaging of a collagen fibril in air to imaging in PBS (pH=7.4), a significant increase of the fibril diameter was observed. The average increase of diameter was found to be (49 +/- 11)% (n=8 fibrils).

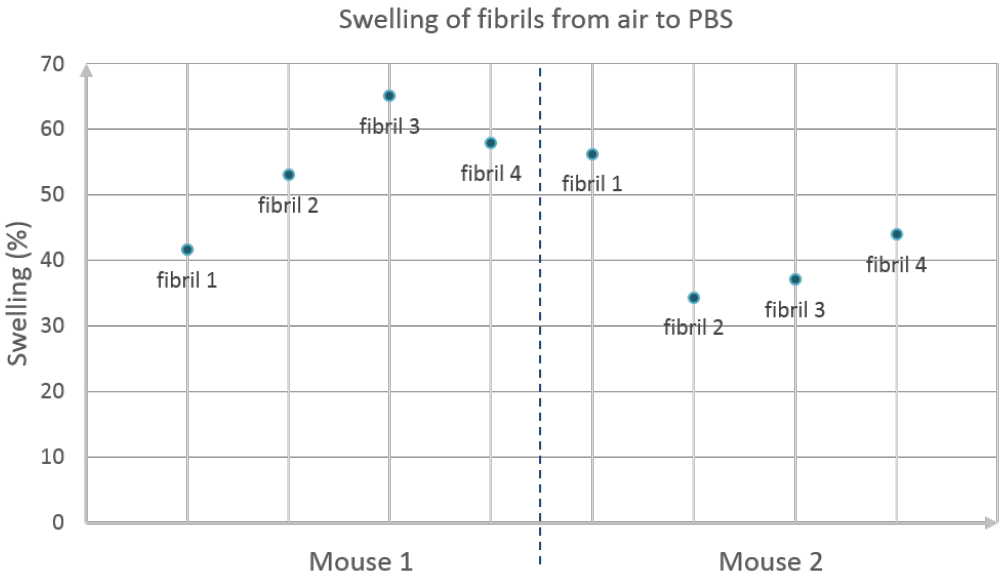

Figure 5.1: Swelling in % of 8 fibrils when hydrated with PBS compared to air dried state.

The swelling ratio does not seem to depend on the fibril diameter in dry state (see Figure 5.12). Erratic fibril height values were deleted by applying a polynomial fit as explained in the previous chapter 4.4.1. This may have slightly modified some values of the crest of the fibril. However, given that at most 10 values of 156 were affected, the effect was deemed insignificant. Differences between the swelling ratio of the tested fibrils may most probably result from fibril to fibril variability. Indeed, the composition of the collagen fibrils and their density may vary. The nature and number of cross linking may as well affect the results. Moreover, D periodic spacings may range from 60 to 73 nm in normal tendon

tissue ([47], [48]). Thus, even when the influence of these parameters on the swelling ratio is not yet known, the hierarchical complexity of the collagen fibrils and the potential for morphological variation with damages have not to be forgotten when providing results.

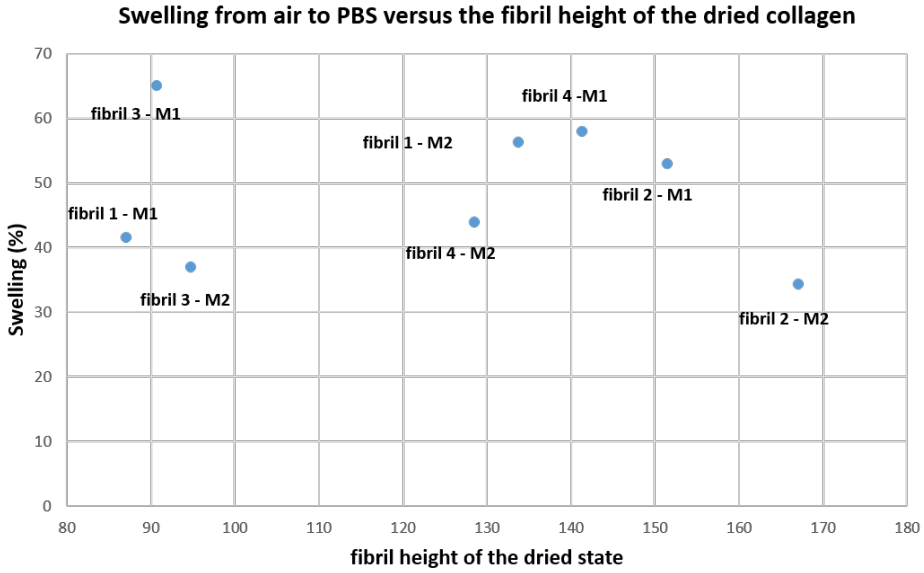

Figure 5.2: Swelling of the 8 fibrils when hydrated in PBS versus the fibril height air dried (M1 for mouse 1 and M2 for mouse 2)

When performing in vitro experiments, considering tissue hydration is essential [31]. Water is one of the main component of the human body. As an example, it constitutes 65% of the total weight of tendons and ligaments. Two forms of water exist: the bound water and the unbound water. Bound water, also known as the water that is not freezable, is present when fibrils are air-dried and is important for the stabilization of the structure of the fibril, and generally of proteins. Unbound water increases upon hydration and is not closely bound to the collagen molecules. The unbound water is responsible for the swelling of the fibril. Assuming a fibril only to be composed of collagen in its air-dried state, the relationship between the volume of water and collagen is given by:

$$\frac{V_{H2O}}{V_{collagen}} = \frac{V_{wet} - V_{dry}}{V_{dry}} = \frac{D_{wet}^2 - D_{dry}^2}{D_{dry}^2} \tag{5.1}$$

From these experiments, the ratio $\frac{V_{H2O}}{V_{collagen}}$ is equal to (1.2 ± 0.2), meaning that there is more water in the collagen fibril than there is collagen content.

5.1.2 Shrinking phenomenon of individual collagen fibril under osmotic pressure

The shrinking phenomenon is obvious in all the fibrils imaged. When increasing the concentration of PEG, the fibril shrinks to reach a new equilibrium. At this moment, the osmotic pressure at the surface of the fibril counters the action of the chemical potential difference and the water stops to flow out of the fibril. The diameter of the fibril decreases progressively while increasing the concentration of PEG. When reaching a concentration in PEG of about 1M or 1.5M, the diameter of the fibril considerably

decreases. At a concentration between 2.6M and 3.5M, changes in diameter are smaller (only few nanometers). Figure 5.3 shows consecutive height topography images of a collagen fibril scanned in air, PBS and at increasing concentrations of PEG.

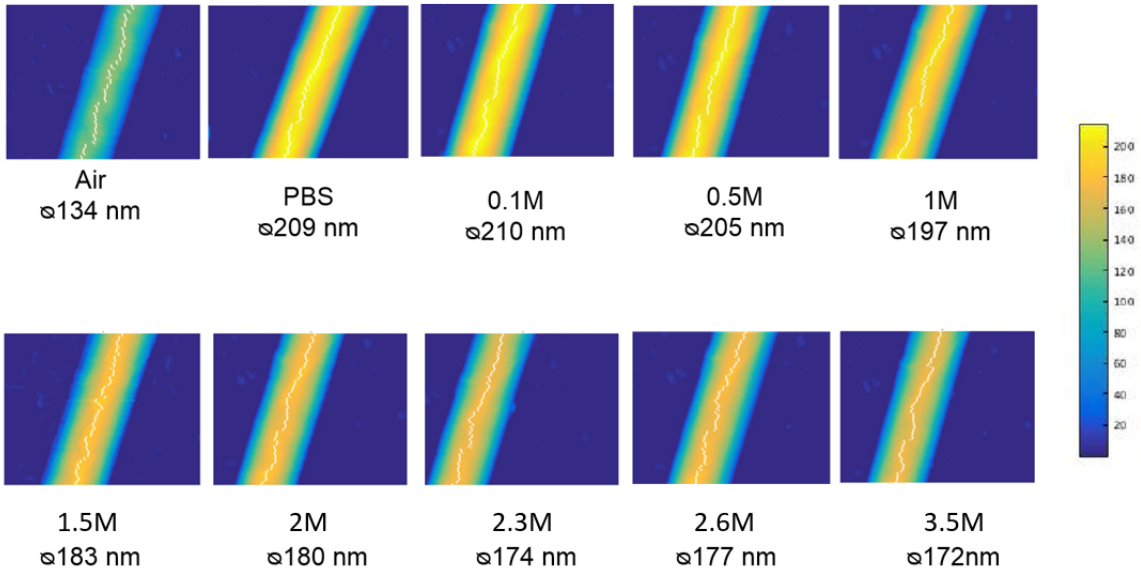

Figure 5.3: Imaging of a selected collagen fibril of mouse 2 in Air, PBS only and PBS with increasing PEG concentration.
The white dots correspond to the maximum height at each profile line i.e. are a measure of the highest contact point between the tip and the fibril (see 4.4.1)

The average decrease of diameter from PBS to the solution in 3.5M PEG was found to be $(16 \pm 4)\%$ (n=8 fibrils, same fibrils as to calculate the swelling ratio from air to PBS).

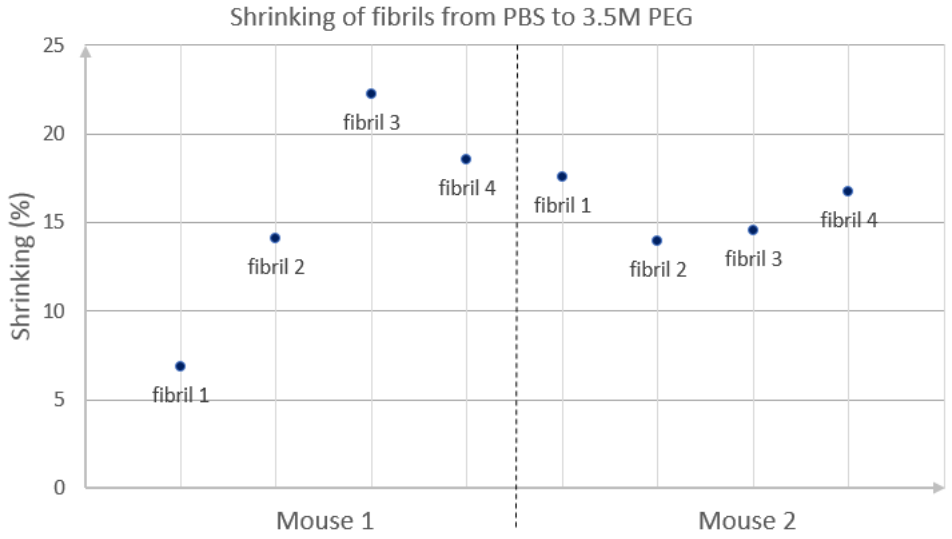

Figure 5.4: Shrinking of 8 fibrils from PBS to the 10M PEG solution

Shrinking ratio in 3.5M PEG is not as high as the swelling ratio in PBS. However, the two

plots (figure 5.1 and figure 5.4) show similar profile: for each sample, the fibrils that swell the most in PBS are also the ones that shrink the most in solutions of increasing PEG concentration. Assuming that the collagen molecule rearranges its structure during hydration and dehydration ([14]) i.e. during swelling and shrinking, the more the swelling the more the structural rearrangement of the collagen molecule, i.e. the more conformational changes that are experienced. Under this hypothesis, the fibrils that swell less and therefore shrink less are those whose collagen molecules are restricted from such conformational changes. The question would then be what restricts collagen molecules from conformation changes. An hypothesis could be that if cross-links, formed between the helical domains, i.e. the AGEs, are present then these could act as barriers to conformational changes. As shown in figure 5.5, the correlation coefficient for the plots of the shrinking in function of the swelling is of 0.99 for the first mouse and 0.89 for the second one. Considering each mouse independently, swelling and shrinking correlates. Nevertheless, when gathering the data of both mice, the correlation coefficient drops to 0.47. The fibrils from the first sample show higher differences in their shrinking from PBS to 3.5M PEG than the ones from the second sample. For the first sample, the maximum variation in swelling is 23% between fibril 1 and fibril 3 and the corresponding maximum variation in shrinking is 15%. For the second sample, the maximum variation in swelling is 22% in between fibril 1 and fibril 2. However, the corresponding maximum shrinking, of less than 4%, is considerably smaller than for the first sample. The calculated slope from the data of the first sample is more than 4 times higher than the one from the second sample. Relation between swelling and shrinking may then vary from one tissue to another. Assuming the hypothesis that cross-links act as barriers to conformational changes, their nature and preferential formation in some tissues, more than in others, may affect the structural and mechanical properties of individual collagen fibril. This may thus affect the properties of the whole tissue or organ.

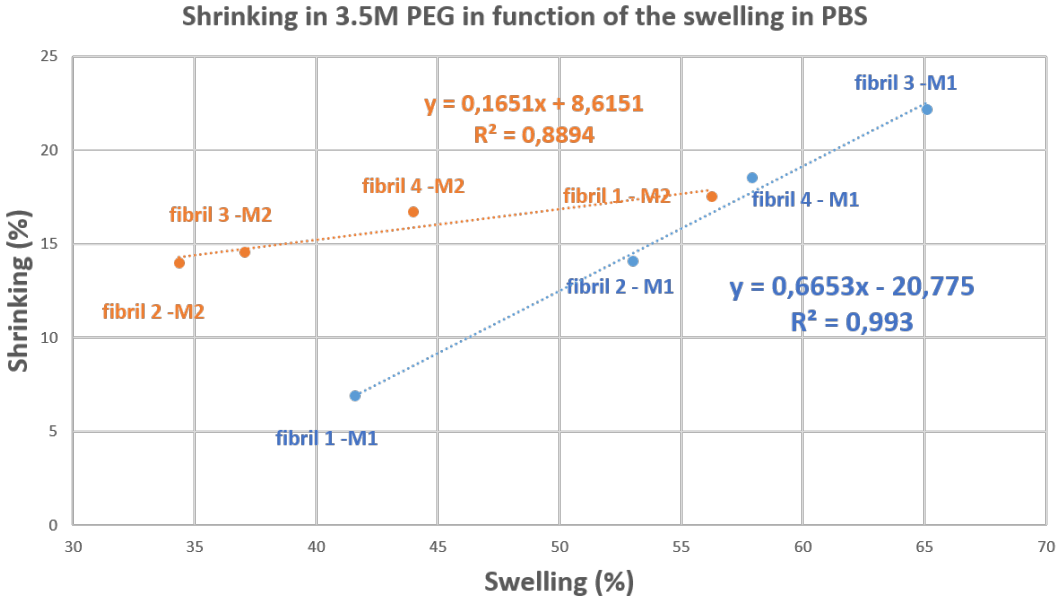

Figure 5.5: Correlation between the swelling from air-dried to PBS and the shrinking from PBS to 3.5M PEG for 8 individual collagen fibrils

For concentrations of 0.1M to 0.5M, the decrease in diameter is only 1-2 %. The decrease

in diameter is larger for concentrations between 1M to 2.6M and then from 2.6M to 3.5M the change in diameter is smaller. Marked changes in the fibril structure occur at concentrations between 1M and 2.6M PEG. Shrinking can be up to 20 % from fully hydrated state and reaches a plateau. This plateau changes from fibril to fibril but is always seen for concentration over 2.6M PEG.

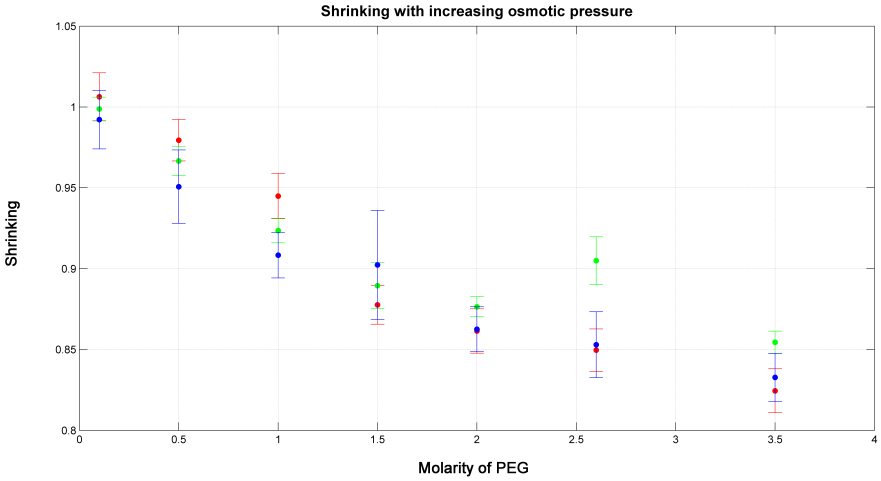

Figure 5.6: Shrinking of 3 independent fibrils for increasing PEG concentration

As an example, figure 5.7 shows cross section profiles recorded at solutions with different concentration of PEG of one fibril (same one as in figure 5.3). The importance of considering the fibril height instead of its width for diameter estimation, due to the envelope effect, can be clearly seen: the transverse value would overestimate the fibril diameter. Main drop in diameter for this fibril is for a concentration in between 1M and 1.5M PEG. The diameter is then slowly decreasing to reach a plateau at a concentration of about 2.6M PEG.

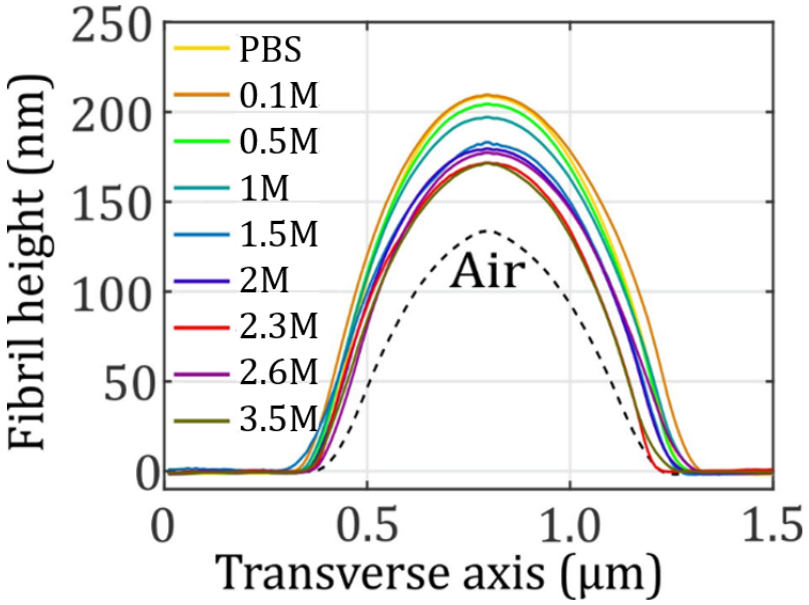

Figure 5.7: Profile analysis of one characteristic fibril

5.1.3 Effect of polyethylene glycol on the indentation modulus

Increasing osmotic pressure results in changes in structural properties but also in mechanical properties. Indeed, nanoindentation unloading curves allow to access transverse elastic modulus values. When increasing the PEG concentration, fibrils appear to become stiffer.

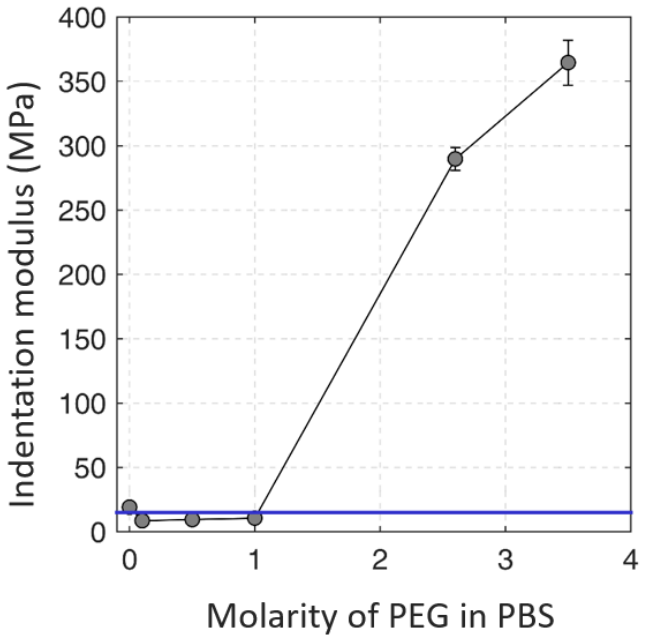

Figure 5.8: Stiffening of one characteristic fibril while increasing osmotic pressure

Figure 5.8 shows the indentation modulus versus the molarity of PEG in PBS. The indentation modulus is 44 times higher in 3.5M PEG than in PBS: it goes from 9 MPa in PBS to 400 MPa in 3.5M PEG. The vast increase observed between 1M and 2.6M for the fibril diameter is also characteristic for the stiffness. Such an evolution of the stiffness under osmotic pressure would considerably change tissue properties.

5.2 Nanotensile testing of collagen fibrils at various osmotic pressures

5.2.1 Stress-strain curves depending on polyethylene glycol solution concentration

Stress-strain curves give information on the stiffness of the fibril. Their slope corresponds to the longitudinal elastic modulus. As for the transverse elastic modulus, stiffening of the fibril is observed for these tests when increasing osmotic pressure.

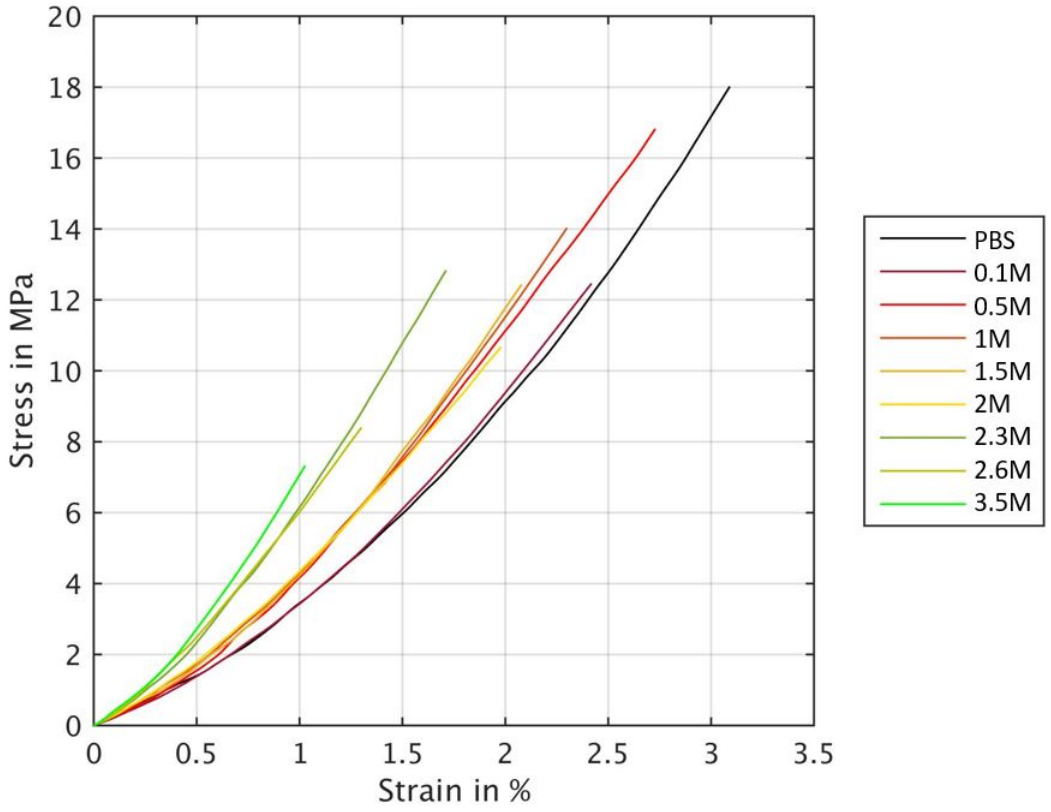

Figure 5.9: Stress-strain of the first cycle of the loading curve for an individual collagen fibril (no resting time) in increasing PEG concentration

In figure 5.9 the contact point is corresponding to the zero point of each curve. It was found prior to the plots in order to display curves from the zero strain to the maximum strain reached. In each solution, each fibril was pulled the same distance and at the same rate of 0.5 μm/s. However, the maximum value of strain reached is changing depending on the solution. With increasing PEG concentration, the fibril is shrinking: its diameter is reducing but its length is also certainly becoming shorter. The shorter and stiffer fibril will thus reach smaller strain in solutions of high PEG concentration compared to ones of low PEG concentration.
This evolution in the slope of the curves could be only by explained by the structural change, i.e. the change in diameter, under increasing osmotic pressure and not an actual stiffening of the fibril. Indeed, stress is dependent of the fibril's area: fibril shrinks when increasing osmotic pressure. However, the force-displacement curves show changes in slope

as it is shown in figure 5.10:

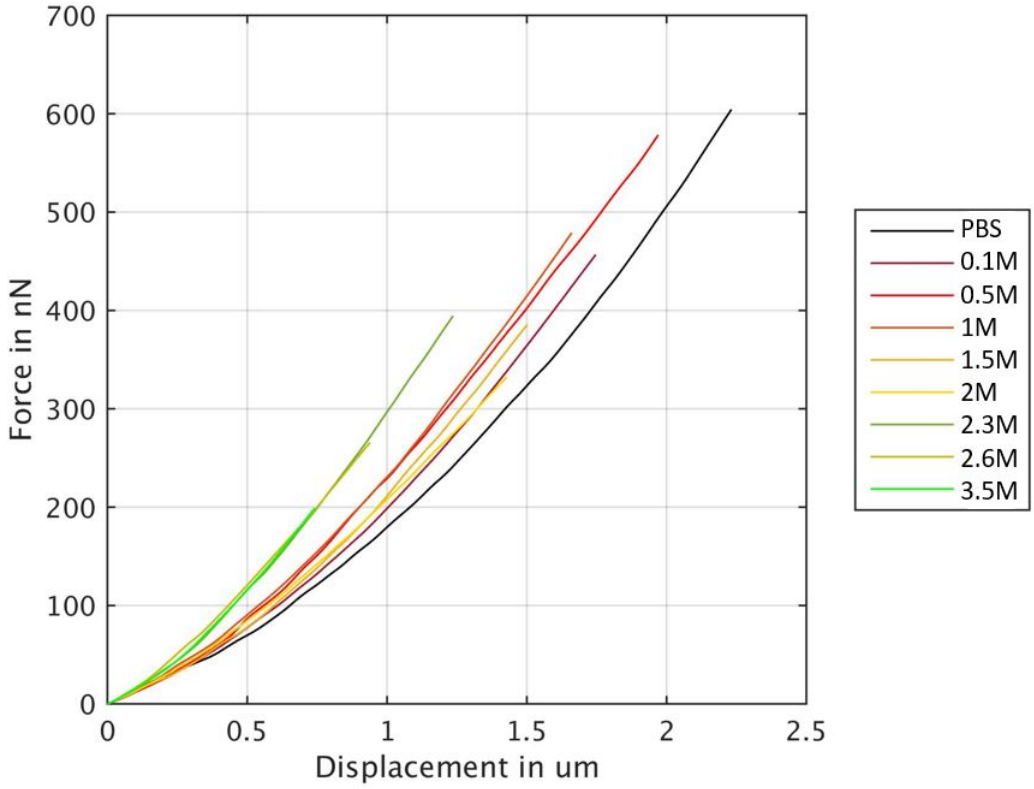

Figure 5.10: Force-displacement of the first cycle of the loading curve for an individual collagen fibril (no resting time) in increasing PEG concentration

These force-displacement curves, where the slope increases with the PEG concentration, confirm the stiffening of the fibril. Structural change can however also increase the stiffness since the interactions between the collagen molecules are increasing.

5.2.2 Effect of solution concentration on fibril longitudinal stiffness

Tangent elastic modulus corresponds to the slope of the stress-strain curve. The maximum strain reached is different from one tested solution to another. It has a minimum value for the solution of 3.5M PEG. This maximum strain at 3.5M PEG is considered in the following graph of the elastic modulus in function of the molarity.

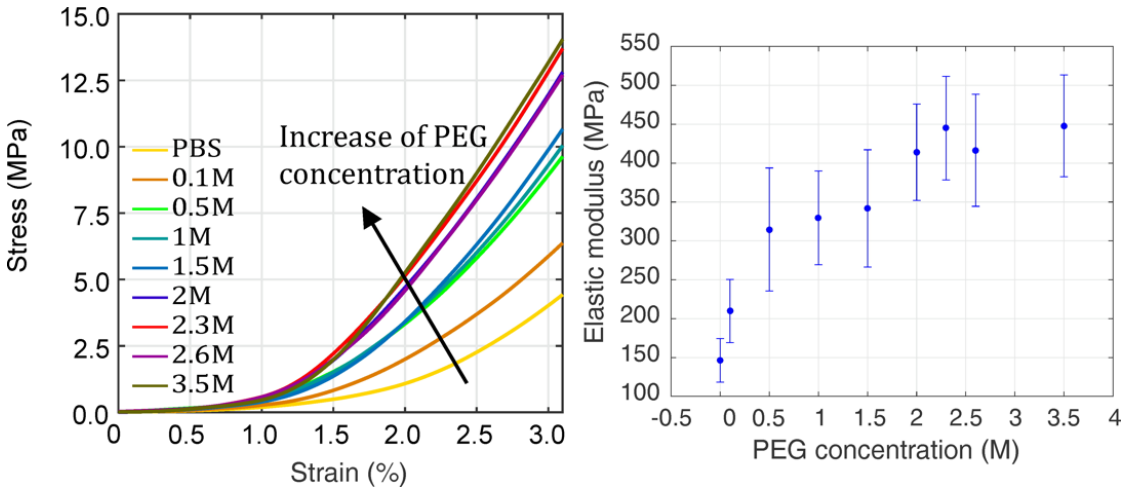

Figure 5.11: Stress-strain curve and elastic modulus value of one fibril for increasing PEG concentration
Elastic modulus values are given at ϵ=3.1%

Longitudinal elastic modulus is increasing by a factor of 3, from 0.15 GPa in PBS to 0.45GPa in 3.5M PEG. Each strain-stress curve is plotted considering the same loading-unloading cycle (the first one). Cyclic loading may induce changes in the collagen fibril stiffness. For this reason, each cycle was considered independently when plotting graphs. Taking the average value on the different cycles may however give a tendency of the evolution of the longitudinal elastic modulus. In figures 5.12 and 5.13, two independent fibrils show an increase of the longitudinal elastic modulus with the PEG concentration. The plots are done at the maximum strain reached by each fibril. The 2 fibrils do not have the same response to increasing osmotic pressure for concentration between 1.5M and 2.6M PEG. As for structural change, such differences may, in part, be explained by variations in composition and density of each individual collagen fibril as well as the nature and number of cross-links. However, the longitudinal elastic modulus has more than doubled for both of the fibrils in 3.5M PEG.

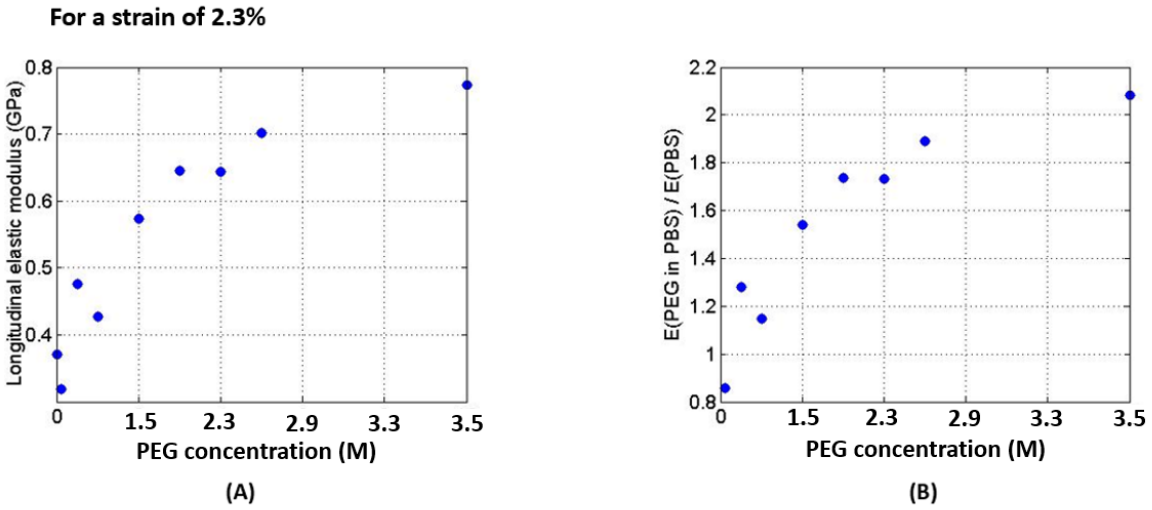

Figure 5.12: Evolution of the longitudinal elastic modulus for fibril 2 at a strain of ϵ=2.3%.
(A) Longitudinal elastic modulus as a function of PEG concentration.
(B) Ratio of the longitudinal elastic modulus in solutions of increasing PEG concentrations over the one in PBS as a function of PEG concentration.

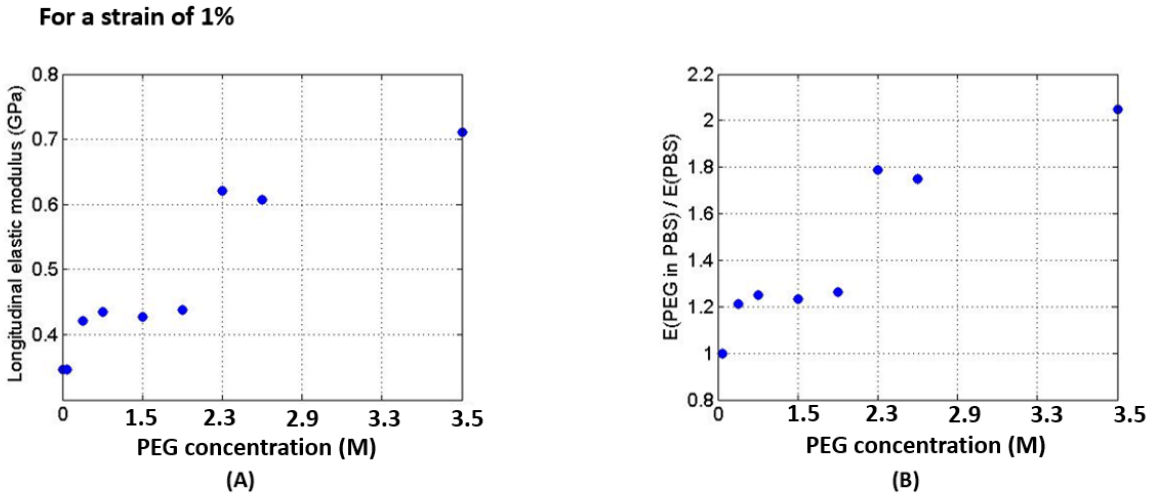

Figure 5.13: Evolution of the longitudinal elastic modulus for fibril 3 at a strain of ϵ=1%.
(A) Longitudinal elastic modulus as a function of PEG concentration.
(B) Ratio of the longitudinal elastic modulus in solutions of increasing PEG concentrations over the one in PBS as a function of PEG concentration.

Plotting the evolution of the elastic modulus at each point recorded, it can be shown that stiffening is a phenomenon observable all along the pulling experiment. The curves in figure 5.14 were low-pass filtered to delete high frequency noise.

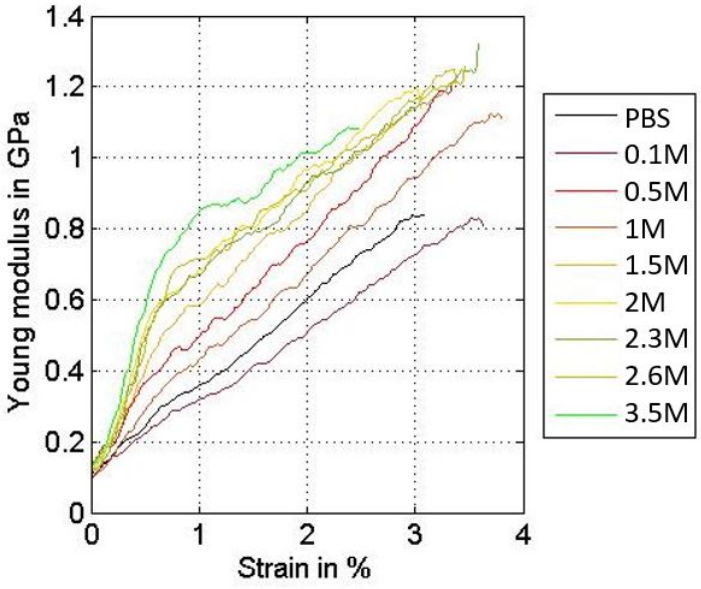

Figure 5.14: Longitudinal elastic modulus from the loading curves of the third cycle in function as a the strain for increasing PEG concentration after low-pass filtering

5.2.3 Mechanical conditioning at the collagen fibril level

For short resting time between loading and unloading cycles, the fibril may not have time to return to its initial state. Assuming this hypothesis, the viscoelastic behavior of collagen may be partly responsible. For cyclic loading of an individual collagen fibril in one solution and without any resting time, mechanical conditioning at the collagen fibril level seems to appear (figure 5.15). The tensile stiffness is indeed dropping which yields to softening of the fibril.

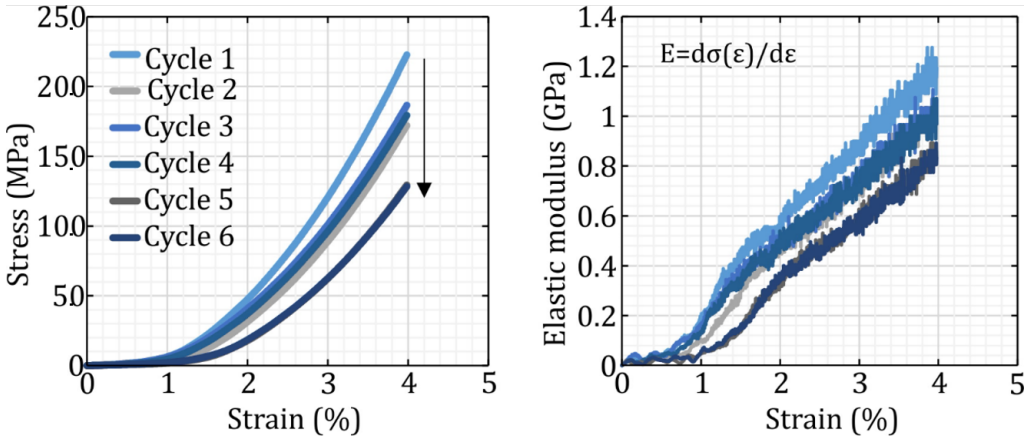

Figure 5.15: Stress-strain loading curves for 6 cycles in 1M PEG solution and corresponding tangent elastic modulus

Mechanical conditioning at the collagen fibril level may depend on many parameters such as the percentage of strain, the number of cycles, the type of collagen involved or the osmotic pressure applied. In figure 5.16, the tangent elastic modulus was plotted at the maximum strain reached for each cycle. Fibril 2 was pulled to a maximum strain of 2.3 % and fibril 3 to a maximum strain of 1 %.

In figure 5.16, the highest values of elastic modulus in each solution are never reached during the last cycle for both fibril 2 and fibril 3. Such results may be explained by a mechanical conditioning at the collagen fibril level. However, the present outcomes are not sufficient to conclude on this question. Indeed, for fibril 2, mechanical conditioning seem to happen in PBS and solutions of PEG concentration less than 2M. However, for solutions of higher PEG concentration, the tangent elastic modulus does not seem to depend on the cyclic loading. For fibril 3, the mechanical conditioning is not obvious for solutions of a PEG concentration under 5M. At the collagen fibril level and under increasing osmotic pressure, different mechanisms may act at the same time and changes in the mechanical and structural properties may influence the response of the fibril. Several leads are below given for further investigations.

Mechanical conditioning may result from uncoiling at the collagen fibril level. A recent study investigates the effect of tensile overload and subsequent unloading on individual collagen fibril. It seems that it caused uncoiling of the collagen helix, positioning local regions of collagen molecules in a stable, denatured state [49]. This phenomenon may be irreversible. Previous studies provide evidence of reversible micro-unfolding of collagen molecules after destabilization of the triple helix ([50]). Mechanical conditioning may be better seen for fibril 2 than fibril 3 since a 1 % higher strain was reached leading to possible reversible uncoiling of the collagen.

Moreover, an increase of the elastic modulus was highlighted for solutions of concentration between 1M to 2.6M PEG (as shown before 5.2.2). Under these particular osmotic pressures, the fibril may be less stable in its structural properties. Smaller variations of PEG concentration may have higher consequences on the fibril and reaching equilibrium may take longer which can influence the mechanical conditioning. When pulling fibril 3 in the solutions of 2.6M and 3.5M PEG, the tangent elastic modulus values are more spread with the cycles than in the other solutions: the tangent elastic modulus drops under the cyclic loading. At higher osmotic pressure, the fibril shrinks and thus its length is also reducing. This decrease may be enough to start to uncoil the collagen when pulling.

These results highlight a potential influence of the cyclic loading, however, more experiments are required to clearly define the process involved. Studying and understanding the mechanical conditioning at the collagen fibril level, including viscoelastic and poroelastic effects, will require to pull many fibrils at different maximum strains and strain rates. The number of loading-unloading cycles per solution could also be increased to be able to compare a larger amount of data. These experiments are beyond the scope of this master thesis due to a lack of time. The pulling experiments take a considerable amount of time, e.g. three days for a single fibril. Investigation leads, as for the potential uncoiling of the collagen, and the limitations of the experiments will be detailed in the following chapter 6.

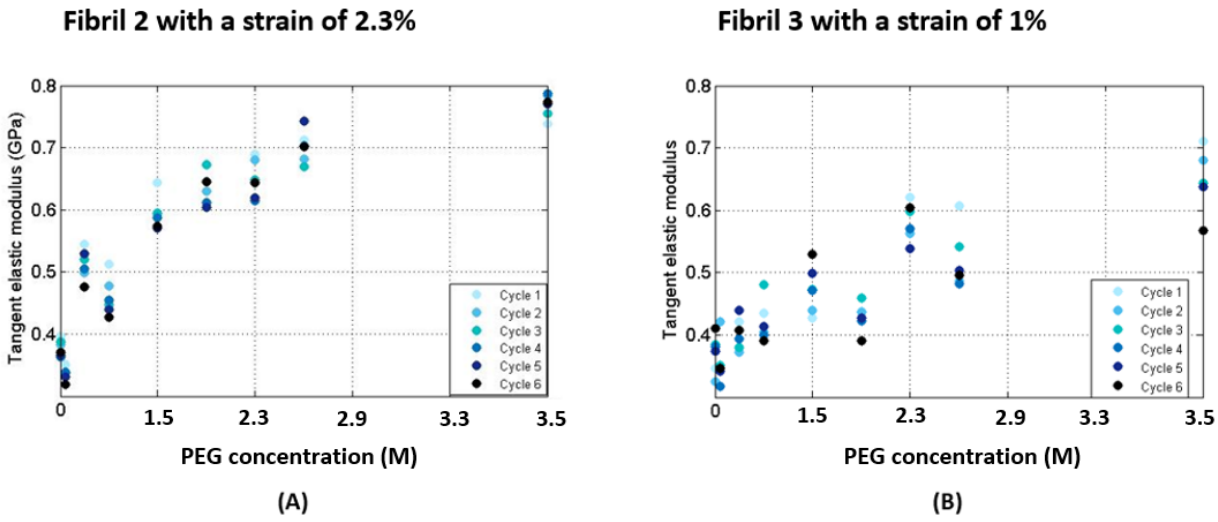

Figure 5.16: Tangent elastic modulus at each cycle in function of the molarity in PEG for 2 collagen fibril. The graph are plotted at the maximum strain reached (i.e. 2.3% for fibril 2 and 1% for fibril 1).

An hypothesis was previously made that mechanical conditioning is, partially happening since the fibril has no time to go back to its initial state. This can be confirmed by performing the same experiments with an increasing resting time.

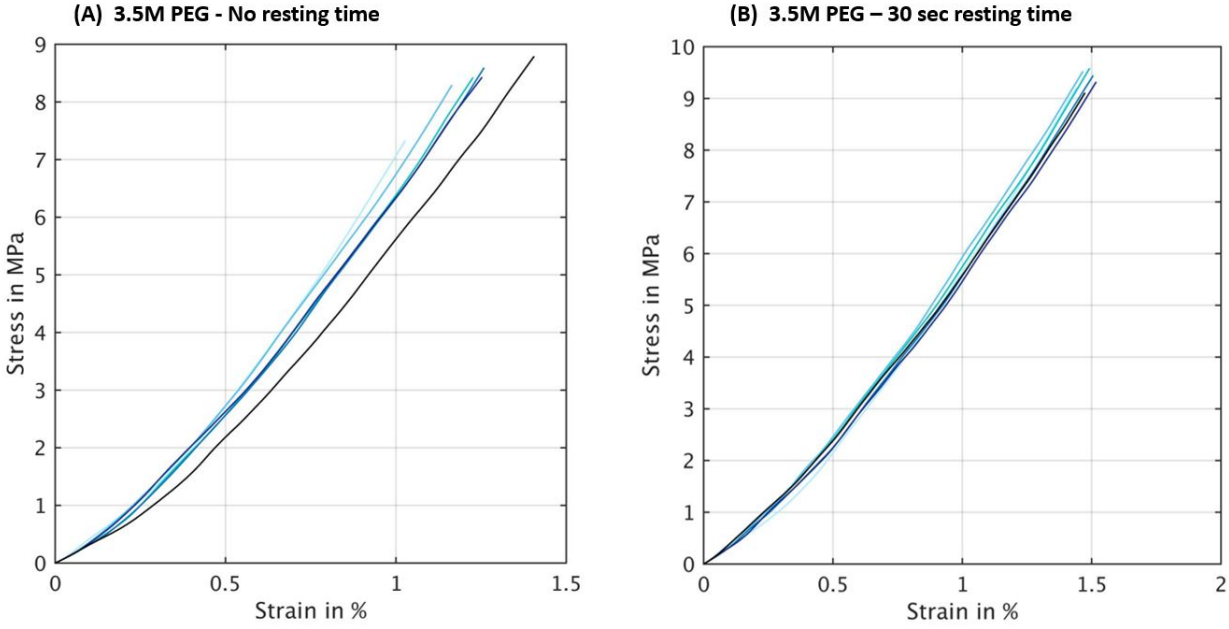

Figure 5.17: Comparison of the stress-strain loading curves for 6 cycles in 10M PEG solution with no resting time (curve (A)) and with 30 sec resting time (curve (B))

As shown in figure 5.17, when waiting 30sec the loading cycle are less spread than without resting time. The fibril seems to partially return to its initial state.

5.2.4 Hysteresis process under increasing osmotic pressure

Viscoelastic behavior at the collagen fibril level leads to hysteresis. 6 loading cycles were performed for each fibril tested. Due to the limitations of the AFM model, the fibril has to be initially pulled. The cycles recorded are thus unloading-loading. In order to obtain the hysteresis curves, the loading data of the first cycle have to be connected to the unloading data of the second cycle. 5 loading-unloading cycles, giving 5 hysteresis curves, are obtained (the first unloading data and the last loading data matching with no other data). However, acquisition had to be stopped in between each of the unloading-loading cycle. The maximum stress value acquired after loading the fibril may thus differ from the maximum stress value acquired at the next unloading of the fibril as shown in Figure 5.18 for a solution of molarity 2.6M PEG in PBS.

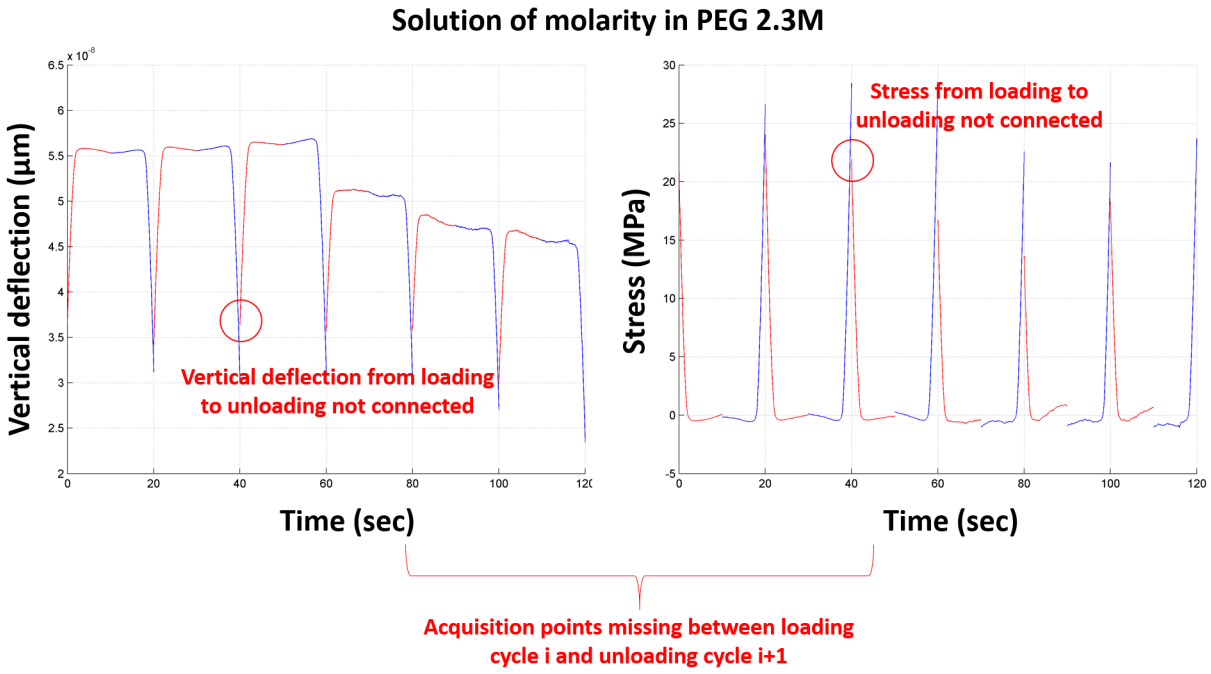

Figure 5.18: Vertical deflection (μm) and stress (MPa) in function of the time for the cycles in 2.6M PEG

In order to connect the loading-unloading curves. The missing acquisition points were estimated using a polynomial fit order 1 calculated on the last points of the unloading curve, as shown in Figure 5.19.

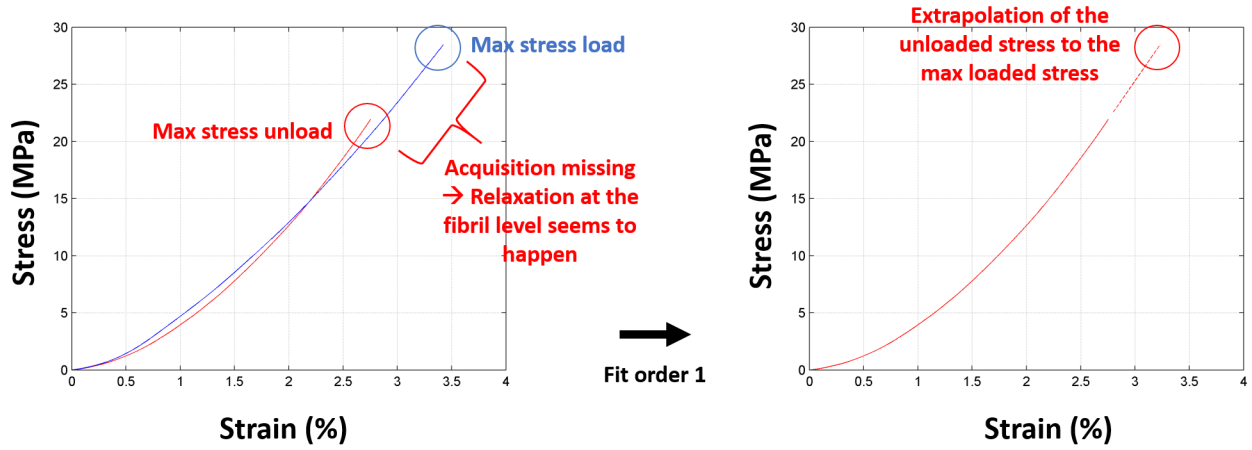

Figure 5.19: Estimation of the non acquired unloading data points with a polynomial fit order 1 for the unloading curve in 2.6M PEG

Connecting the loading and unloading curves without considering the missing data points results in an artifact. Extrapolation of the last unloading points seem to give a more reliable result of the hysteresis at the collagen fibril level.

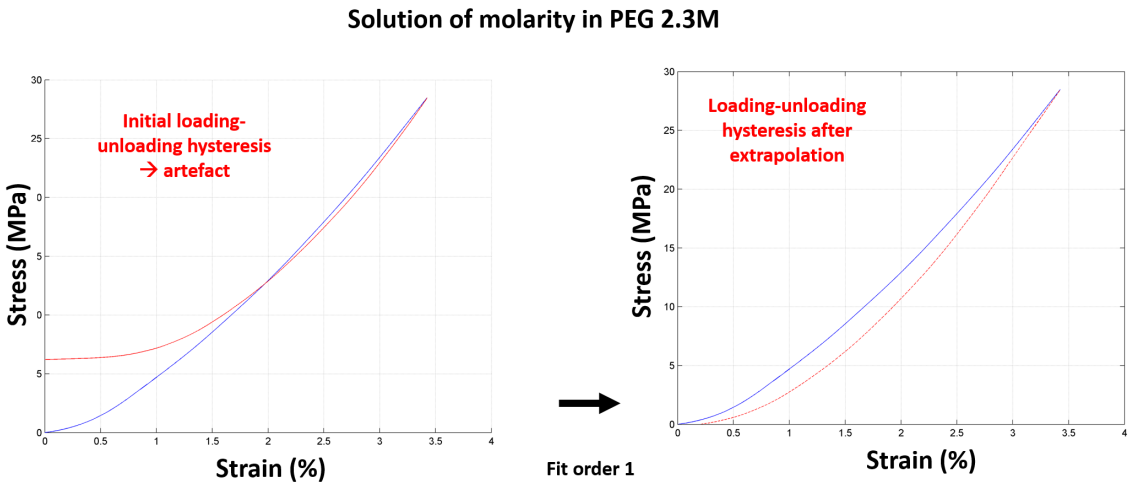

Figure 5.20: Hysteresis curves before and after the extrapolation of the unloading missing data points for a solution of 2.6M PEG (cycle 2)
in blue: loading - in red: unloading

After repeating the same processing on the loading-unloading curves in each tested solution, the hysteresis curves are obtained. Hysteresis is clearly seen at the collagen fibril level. The fibril needs more time to reach again its initial state.

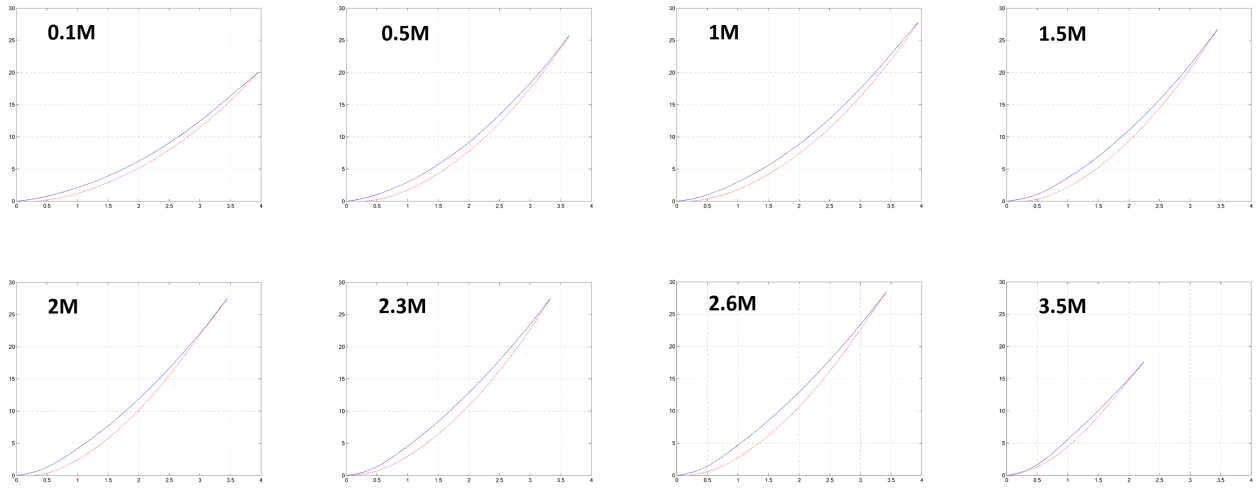

Figure 5.21: Hysteresis curves in increasing osmotic pressure for the second loading-unloading cycle
in blue: loading - in red: unloading

The stress values were plotted in function of the time for all the cycles in solution of increasing PEG concentration. At low osmotic pressure, the fibril seems to get stiffer during the time where no data were acquired. Indeed, considering the second loading-unloading cycle in Figure 5.22, the maximum loaded stress is 16 MPa while the maximum unloaded stress is 20 MPa for a solution of 0.1M PEG. While increasing the osmotic pressure, the fibril does not seem to show preferential stiffening or relaxation before the resumption of the acquisition. For higher osmotic pressure (as displayed in Figure 5.19 and Figure 5.22), relaxation seems to happen at the collagen fibril level. The maximum stress reached in 2.6M PEG was 28 MPa for the loading of cycle 2 while the maximum stress acquired when unloading the fibril again is 22 MPa. Osmotic pressure may thus affect the response of individual collagen fibril to cyclic loading. An hypothesis is that, at low PEG concentration, ions may be removed from the fibril when pulling. The osmotic pressure applied may not allow these ions to directly go back into the fibril. Consequently, at the end of the loading, the fibril may continue to get stiffer, even after stopping the acquisition. When increasing the osmotic pressure, the fibril gets stiffer and its length may decrease. For the same stress felt by the fibril, smaller strain are reached in solution of higher PEG concentration, from 4 % in 0.1M to less than 3.5 %in 2.6M. In 3.5M PEG, the maximum strain, less than 2.5 %, and stress, more than 17 MPa, reached during the cycles drops compared to the ones in solutions of inferior PEG concentration (see Figure 5.21). At higher PEG concentration, the smaller and stiffer fibril may start to uncoil. This hypothesis was previously made to explain a possible mechanical conditioning under cyclic loading. In the time lapse between the end of the loading acquisition and the beginning of the next unloading acquisition, relaxation may happen at the collagen fibril level.

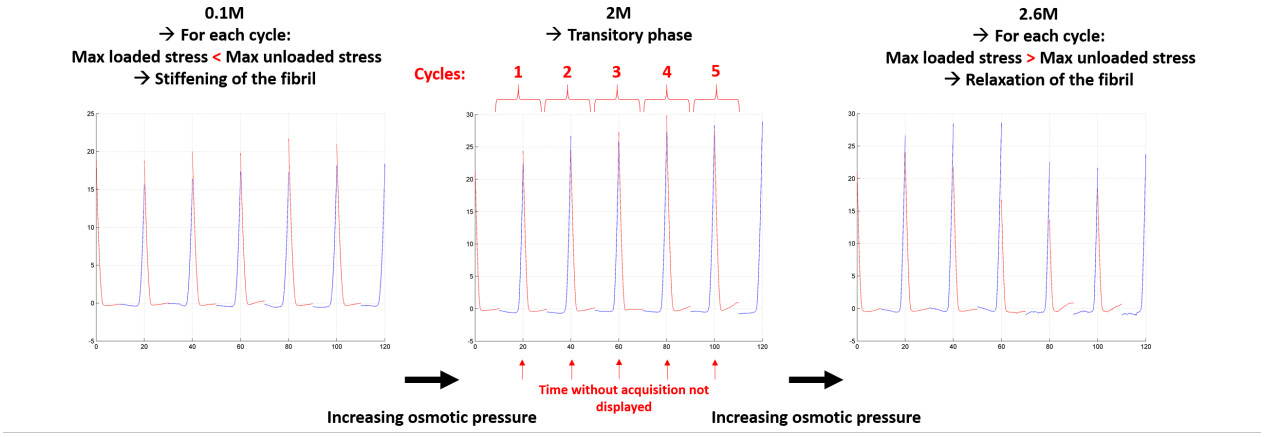

Figure 5.22: Evolution of the stress felt by the collagen fibril during cyclic loading with increasing the osmotic pressure
in blue: loading - in red: unloading

5.2.5 Effect of the strain rate on the implementation of stress-strain curves

To control the strain rate during experiments, the speed of the Z-piezo approach and retract steps has to be changed. The strain rate is defined as :

$$\dot{\epsilon} = \frac{v(t)}{L_0} \tag{5.2}$$

With v(t) the speed of the Z-piezo and L_0 the zero strain fibril length as before.
As expected increasing the strain rate is leading to the stiffening of the fibril. This phenomenon is seen in PBS as in solutions of increasing PEG concentration.

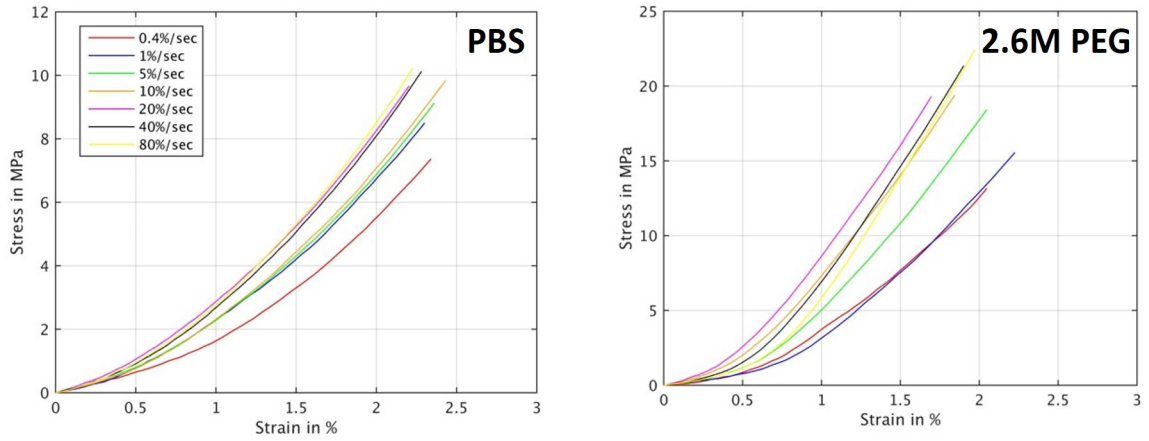

Figure 5.23: stress-strain loading curves for the first cycle with increasing strain rate in PBS and 2.6M PEG

In the figure 5.23, a strain rate of 80%/s is corresponding to a pulling at a speed of 99.2 μm/s. The duration of the loading and unloading steps were then of 0.05 sec. Typical movements in tendon are quite fast and physiological strain rates achieve in running may

range from 15%/s to 70%/s [51]. Experiments done on tendons from equine foreleg show even higher values with strain rates up to 200%/ [52]. Stiffening at the collagen fibril level is clearly seen in both of the solutions. However, it can be noticed that strain rate dependency in tendon is not as high as it is in other soft tissues [53]; the influence of this parameter was then not deeper studied during this master thesis.

Chapter 6

Discussion and Conclusions

6.1 Experimental outcomes of nanoindentation and nanotensile experiments

Nanoindentation and nanotensile experiments were performed on an atomic force microscope. They highlight the effect of increasing osmotic pressure level on individual collagen fibril. The effect of increasing osmotic pressure exerted by the proteoglycans and glycosaminoglycans was simulated by increasing the concentration of polyethylene glycol (PEG) in PBS solution from 0.1M to 3.5 M. Additionally, imaging in air was also conducted prior to nanoindentation experiments. While increasing the PEG concentration in the solution, stiffening of the collagen fibrils is observed in both the transverse and the longitudinal direction. Under the same conditions of increasing osmotic pressure, a decrease of the diameter of the fibril was also measured. A schematic representation on the effect of osmotic pressure on the structure of the fibril is shown in Figure 6.1.

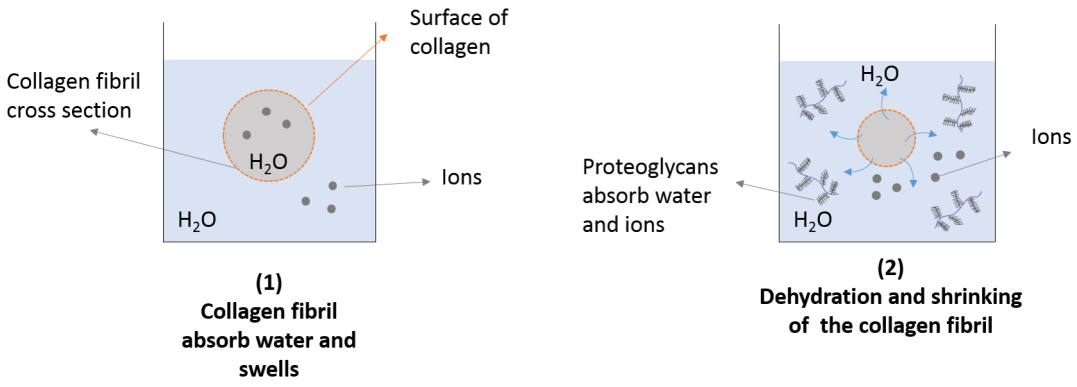

Figure 6.1: Principle of osmotic pressure on an individual collagen fibril.

From a structural point of view, swelling of the fibril in PBS compared to air and shrinking in increasing PEG concentration solutions compared to PBS are observed. These processes are a function of the osmotic pressure applied as a result of hydration (when swelling) and dehydration (when shrinking) of the fibril. When adding PBS to an air-dried fibril, the concentration in ions and thus the chemical potential are higher in the fibril than outside. Collagen is, indeed, charged and extracts water and the counter-ions. Water

is absorbed by the fibril under the effect of a concentration gradient; this is called osmosis. Equilibrium is reached when the flow stops: osmotic pressure counteracts the effect of the chemical potential difference. Swelling measured in PBS via the diameter increase from the air-dried state is $(49 \pm 11)\%$. Shrinking of the fibril results from the same osmosis process. The proteoglycans absorb both the water and the salt ions leading to the dehydration of the collagen fibril. Indeed, the sat ions have a higher affinity to the proteoglycans. The ECM is composed of high negative charged molecules, i.e. the proteoglycans and glycosaminoglycans, and of collagen, as in tendons. For the experiments, an increase in PEG concentration was used to represent an increase of the amount of proteoglycans in the ECM. When increasing the PEG concentration of the solution, in which the fibril is submerged, the concentration of salt ions is higher outside than inside the fibril. Water is thus removed from the collagen fibril and shrinking of the fibril is observed. Shrinking was up to 20%, with 100 % at PBS, with a mean value of $(16 \pm 4)\%$ when in 3.5M PEG. Additionally, swelling and shrinking seem to correlate when considering the samples independently. The higher the swelling, the higher the shrinking is.
From a mechanical point of view, shrinking is associated to stiffening of the fibril in both the transverse and the longitudinal direction. The transverse elastic modulus can be about 44 times higher from fully hydrated state to 3.5M PEG in PBS as a result of increase in packing density due to a decreased intermolecular lateral distance. Tissue properties could thus considerably change under increasing osmotic pressure. For concentrations in between 1M and 2.6M PEG, shrinking and stiffening change quickly. A significant decrease in the diameter of the fibril as well as an increase in stiffness was noticed. The diameter seems to finally reach a threshold value for solution of 3.5M PEG. Longitudinal elastic modulus increases by a factor of 3 at the highest osmotic pressure applied. Higher rate of stiffening is again observed for PEG concentration in between 1M and 2.6M. Shrinking of the fibril under osmotic pressure also results in a decrease in the length of the fibril, not quantified during this study.

Influence of parameters such as resting time and strain rate were also tested. In each solution and for each parameter tested, 6 cycles (loading and unloading) were implemented. While increasing the osmotic pressure, stiffening of the fibril was observed as for the nanoindentation experiments. Ultimate strain of about 10% to 12% can be reached in tendons [54]. Strain within collagen fibrils is, however, always considerably smaller than in the whole tendon [55]. Strain up to 4% were reached during the experiments to be coherent with physiological strains. Fibrils were not damaged as they are capable of reversible deformation with a resilience of approximately 90% [56].
Mechanical conditioning at the collagen fibril level seems to occur under cyclic testing: the fibril becomes softer. However, the study of this phenomenon and the role of osmotic pressure need to be further investigated.
Hysteresis seems to happen during cyclic loading, in part due to the viscoelastic behavior of the collagen fibril. It is however difficult to conclude on the influence of the PEG concentration on the hysteresis area.
An other test was focused on the influence of the strain rate. Most experiments were done at low strain rate of about 1%/sec by setting the velocity of the Z-piezo to 0.5μm/sec tough physiological strain rate are higher in tendons. Influence of increasing strain rate was tested on one of the fibril. It leads to stiffening and does not seem to be dependent of the osmotic pressure. Investigations on the effects of strain rate on mechanical and failure properties were carried on in the last decades at the macroscale and the microscale, and

more recently at the nanoscale. With higher strain rate, tendons in isolation store more energy, require more force to rupture and can undergo greater elongation [57]. Studying the responses of the individual collagen fibril under physiological strain rate can provide a deeper understanding of variations in the physical properties of the fibrils and how energy is transmitted from nanoscale to macroscale.

6.2 Experimental limitations and further development

Within this master thesis, protocols for the AFM experiments were developed and/or adjusted to provide satisfactory results in terms of accuracy and reproducibility.

Nanoindentation experiments using AFM provide accurate results for imaging in air as well as in aqueous solutions. In high PEG concentrations, liquid is more viscous and approaching the surface with precision is more difficult. During shrinking the molecules that compose the fibril change their conformational structure. For every conformational change, i.e. for every concentration of PEG, ions exposed to the surface of the fibril may be different. This may affect the contact point and AFM imaging due to changes in the forces interactions at the surface. However, the error in the actual contact point can be neglected since it is small compared to the shrinking and may be less pronounced for force indentation experiments. It was thus chosen to perform AFM nanoindentation using the QI mode. Imaging is however taking longer than in standard tapping (or AC) mode. More artifacts can appear, in particular due to the higher velocities of the cantilever towards the surface. Repeatability is easy to implemented for such experiments. Imaging can, however, not be automated and thus gathering a large amount of data requires time.

In the case of nanotensile experiments, AFM is not initially made for such experiments. Gluing and ungluing of the fibril requires experience with an approximate rate of success of 50%. The epoxy can sometimes not be detached from the surface without enough pre-cure. The fibril may also break at one end before starting the experiment. Use of micromanipulators might help to perform this delicate task within a reasonable time-frame and with more efficiency. At the moment, preparation of a single fibril for pulling takes 2 to 3 days. Nevertheless, the tensile experiment itself is successful almost every time; the most difficult part is to locate the zero strain length. A large number of experiments can be implemented per fibril. Loading and unloading are generally quick, if no or only a short resting time is applied. The fibril is, however, most likely kinked on the points of contact with the epoxy. This will likely result in higher stresses in these locations. Switching from one solution to another is currently done using pipettes and may be further improved using a fluid cell that allows inlet and outlet of fluid using syringe pumps. Increase of the precision of the experimental protocol could also be a way of studying effects of smaller PEG variations in solutions. The actual protocol allows to increase the concentration by 0.5M PEG and is not precise enough for smaller addition in PEG. However, it may be that, for smaller variations of the PEG concentration, the effect is not as prominent. Therefore, it may be difficult to conclude on the changes that could be seen in the measured values. They may be due to an actual effect of the PEG concentration or simply result from imprecision of the experimental protocol.
The main drawback of the use of this AFM model for nanotensile experiments is that the Z-piezo, when not in approach, is always retracted. From its zero-strain length, in the Z-piezo retracted position, the fibril can not be pulled anymore. The only way to do the tensile test is to initially pull on the fibril and then to extend the Z-piezo to reach back

the zero strain length. Cycles are, thus, not loading and unloading but the reverse. When studying the hysteresis this was taken into account to associate the appropriate loading and unloading curves in order to respect the continuity of the experiment (i.e. loading curve of the first cycle with unloading curve of the second cycle for example). However, this introduces specific artifacts. When connecting the loading and unloading curves, data are missing before the restart of the acquisition. In order to connect the loading and unloading curves, an extrapolation of the missing points was done. It seems that, at higher PEG concentration, the collagen fibril may start to uncoil. During the time lapse between the end of the loading acquisition and the beginning of the next unloading acquisition, the stress felt by the fibril is decreasing. However, in order to fully understand the influence of the osmotic pressure on cyclic loading, additional experiments are needed.
The experiments are all performed in displacement control, which is easier to perform as the displacement of the Z-piezo is set to reach the zero-strain length of the fibril. It provides coherent results, and differences in mechanical properties of the fibril from PBS to solutions of increasing PEG concentration are highlighted. It would also be interesting to perform force controlled experiments after defining a relevant force value for the zero strain length. In a specific experiment [27], it was defined as the moment where the stress first exceeded 200 kPa. The choice of this value could, however, be discussed. Comparing the results from displacement controlled and force controlled nanotensile experiments is a good opportunity to study the advantages and drawbacks of both methods. Force controlled experiments could not be performed during this master thesis due to technical issues which will need to be resolved in future experiments. The current version of the software is, indeed, not allowing to perform such experiments.

The magnitude of osmotic pressure may not be physiological relevant. At the moment, the osmotic pressure is estimated to be about 25 MPa, for the highest concentration of PEG, from existing data ([58]). The use of an osmometer could be a good way of evaluating osmotic pressure values corresponding to each PEG concentration. By linking these values of pressure to the ones exerted by the proteoglycans in the ECM, a precise representative physiological responses of the fibrils to osmotic pressure could be established.

Shrinking at the collagen fibril level should occur in the human body as the result of the action of proteoglycans. Depending on their concentration, structural properties may change more or less widely. The amount of water that the fibril can hold is most likely to affect the magnitude of shrinking. Cross-linking may also play an important role in the hydration of the fibril. Cross-linking may differ between fibrils as a result of their structural composition. A fibril can be made of many different collagen molecule types. In tendons, the fibrils are amalgamations of collagen type V, III and a large amount of collagen type I to ensure the structural and the functional stability of the whole tissue. The relative amount of collagen type I and III and other molecules, as the decorin, may change between tissues, and perhaps between different fibrils of the same tissues. Therefore, the composition of the fibrils, may be related to changes in its swelling and shrinking behavior. The differences observed may also depend on possible damages at the surface of the fibril.

Transverse and longitudinal elastic modulus respectively obtained from the nanoindentation and nanotensile experiments are different in terms of values due to the anisotropic nature of collagen. However, stiffening under increasing osmotic pressure was clearly demonstrated in both cases. A larger increase was particularly seen for concentration in PEG ranging from 1M to 2.5M. Adding solutions in the study in between these particular concentrations would provide more details on both the structural and mechanical properties of the fibril.

Potential mechanical conditioning at the collagen fibril level was also noticed. Such a phenomenon can be seen on the whole tendons ([59], [60]) but has so far not shown at the nanoscale. Previously, studies were carried on tensile properties of partially hydrated individual collagen fibril ([11]). Using a microelectromechanical systems platform, stress-strain curves were obtained from fibril tested under uniaxial tension. Decrease of the yield point with cyclic loading was highlighted ([11]). However, this decrease was defined as a consequence of accumulation of damages due to the high strain reached. Defining the mechanical conditioning and its limits at the collagen fibril level is difficult. Many parameters can be involved in this process such as the susceptibility of cyclic fatigue, the maximum strain reached or the effect of water or the osmotic pressure applied. Implemented a larger number of cycles in different medium on a single fibril is required to have a deeper understanding of what is happening in the fibril and the possible link to osmotic pressure. Uncoiling of collagen molecules may happen and modify the response to load of the fibril. A study carried on the subject ([49]) shows that tensile overload reduces the enthalpy of denaturation of tendons, i.e. the variation in enthalpy required to denature one Mole of compound, and increases the amount of collagen solubilized from tendons during trypsin digestion. Such results point out the fact that the helix of collagen molecules can uncoil when overloading, placing the collagen fibril in a stable, denatured state. The conformational freedom of collagen molecules is increasing leading to a reduction of thermal stability and reversible micro-unfolding of the collagen helix [54]. When hydrated, the collagen fibril contains a large amount of water which can flow out of the fibril when loading and flow back in when unloading, collagen being here poro-elastic. Under high osmotic pressure, the fibril is stiffer and contains less water, which can result in a progressive unfolding and possible damages. Refolding may require time and thus may be impossible to achieve under cyclic loading without any resting time. Mechanical conditioning would, in this case, not necessary be seen if the collagen fibril is staying in its current denatured state (i.e. neither refolding or further unfolding).

Experiments chosen in this study have limitations and need to be carried on further in the future. Nevertheless, it is possible to speculate about the general structural and mechanical response to osmotic pressure of an individual healthy collagen fibril. Whereas collagen fibrils are passive proteins, cells are able to dynamically alter their environment. Although in general collagen cross-linking may lead to stiffer collagen fibrils, the process of cross-linking is time consuming. Cells may use the osmotic pressure-related mechanical tunability of collagen fibrils to alter the mechanics of collagen in a short period of time. To achieve that, cells would secrete proteoglycans increasing locally the osmotic pressure and hence increasing structural stiffness of their surrounding. According to our experiments, this happens within some minutes. It is a much faster way to modulate the mechanical properties of the tissue, although producing proteoglycans also takes time for the cells, than, for example, changing the biochemistry of collagen i.e. increasing the enzymatic cross-links. It is also very important that this is reversible. Osmotic pressure may be one major contributor to this adaptation. Research can be pushed further to study effect of parameters peculiar to the fibril itself as collagen cross-linking or responses of damaged fibril under varying osmotic pressure. Performing additional experiments would be necessary to fully understand how osmotic pressure can tune the properties of collagen fibrils.

6.3 Conclusion

The aim of this master thesis was to investigate structural and mechanical properties of individual collagen fibrils under increasing osmotic pressure. AFM is a well documented method for imaging and nanoindentation. Experiments are time consuming but easy to repeat. Nanotensile tests using an AFM was a harder task to implement. However, several collagen fibrils could be pulled to strain up to 4%. I particularly would like to thank René B. Svensson for his help and information provided on the subject ([27]). Being able to access results from both nanoindentation and nanotensile experiments provides more significant results: both transverse and longitudinal directions could be studied. Collagen fibril is, indeed, an anisotropic biological structure. Stiffening of the fibril was highlighted in both cases with an increase in the elastic modulus and stiffness. The transverse elastic modulus was found to be 44 times greater from PBS to 3.5M PEG in PBS while the longitudinal elastic modulus increased by a factor of 3. Shrinking of the collagen fibril is happening under the same experimental conditions, which may also have an effect on the mechanical properties due to interaction between collagen molecules.
From this master thesis, the main take home message is the preferential tuning using osmotic pressure of the structure and mechanics of tissue scaffolds, the collagen fibrils. By producing proteoglycans, the cells may quickly change the osmotic pressure in the ECM in order to modulate mechanical tissue properties over a large range of elasticity values. Particular needs of a tissue under specific physiological conditions may then be satisfy.

Bibliography

[1] James H.C. Wang. Mechanobiology of tendon. *Journal of Biomechanics 39*, pages 1563–1582, 2006.

[2] K Misof, W J Landis, K Klaushofer, and P Fratzl. Collagen from the osteogenesis imperfecta mouse model (oim) shows reduced resistance against tensile stress. *The Journal of Clinical Investigation*, 100:40–45, 1997.

[3] HS Gupta, J Seto, W Wagermaier, P Zaslansky, P Boesecke, and P Fratzl. Cooperative deformation of mineral and collagen in bone at the nanoscale. *PNAS*, 103:17741–17746, 2006.

[4] Peter Fratzl. Cellulose and collagen: from fibres to tissues. *Current opinion in colloid & interface science 8 (1)*, pages 32–39, 2003.

[5] Orestis G. Andriotis. *Nanostructure and mechanics of collagen fibrils from osteogenesis imperfecta mice and chronic asthma assessed with atomic force microscopy.* PhD thesis, University of Southampton - Faculty of engineering and the environment, november 2013.

[6] B. Depalle, Z. Qin, S.J. Shefelbine, and M.J Buehler. Influence of cross-link structure, density and mechanical properties in the mesoscale deformation mechanisms of collagen fibrils. *Journal of the Mechanical Behavior of Biomedical Materials*, 2014.

[7] Orestis G. Andriotis , Wiparat Manuyakorn , Jurgita Zekonyte , Orestis L. Katsamenis , Sebastien Fabri , Peter H. Howarth , Donna E. Davies , Philipp J.Thurner. Nanomechanical assessment of human and murine collagen fibrils via atomic force microscopy cantilever-based nanoindentation. *Journal of the mechanical behavior of biomedical materials 39*, pages 9–26, july 2014.

[8] Chi H. Lee , Anuj Singla , Yugyung Lee ,. Biomedical applications of collagen. *International journal of pharmaceutics 221*, pages 1–22, june 2001.

[9] D.F. Holmes, C.J. Gilpin, C. Baldock, U. Ziese, A.J. Koster, and K.E. Kadler. Corneal collagen fibril structure in three dimensions: structural insights into fibril assembly, mechanical properties, and tissue organization. *Proc.Nat. Acad. Sci.*, 98:7307–7312, 2001.

[10] M. P. E. Wenger , L. Bozec , M. A. Horton , P. Mesquida. Mechanical properties of collagen fibrils. *Biophysical journal 93*, pages 1255–1263, 2007.

[11] Z. L. Shen , M. R. Dodge , H. Kahn, R. Ballarini , S. J. Eppell. Stress-strain experiments on individual collagen fibrils. *Biophysical journal 95*, pages 3956–3963, 2008.

[12] R.B. Svensson, H. Mulder, V. Kovanen, and Magnusson S.P. Fracture mechanics of collagen fibrils: Influence of natural cross-links. *Biophysical journal*, 104(11):2476–2484, 2013.

[13] Y Lu, K.H Parker, and W Wang. Effects of osmotic pressure in the extracellular matrix on tissue deformation. *Philosophical Transactions of the Royal Society of London A: Mathematical, Physical and Engineering Sciences*, 364(1843):1407–1422, 2006.

[14] A. et al. Masic. Osmotic pressure induced tensile forces in tendon collagen. *Nature Communications 6:5942*, 2015.

[15] P. Fratzl, H. S. Gupta, E. P. Paschalis, and P. Roschger. Structure and mechanical quality of the collagen-mineral nano-composite in bone. *J. Mater. Chem.*, 14:2115–2123, 2004.

[16] M.E. Launey, P.-Y. Chen, J. McKittrick, and R.O. Ritchie. Mechanistic aspects of the fracture toughness of elk antler bone. *Acta Biomaterialia*, 6:1505–1514, 2010.

[17] P. Fratzl. Cellulose and collagen: from fibres to tissues. *Current opinion in colloid & interface science*, 8:32–39, 2003.

[18] Francisco S. A. Cavalcante, Satoru Ito, Kelly Brewer, Hiroaki Sakai, Adriano M. Alencar, Murilo P. Almeida, José S. Andrade, Arnab Majumdar, Edward P. Ingenito, and Béla Suki. Mechanical interactions between collagen and proteoglycans: implications for the stability of lung tissue. *Journal of Applied Physiology*, 98(2):672–679, 2005.

[19] Peter Fratzl. *Collagen Structure and Mechanisms*. Springer Science+Business Media, LLC, 2008.

[20] P. Kannus. Structure of the tendon connective tissue. *Scandinavian Journal of Medicine and Science in Sports 2000*, pages 312–320, 2000.

[21] The Editors of Encyclopedia Britannica britannica.com. Tendon.

[22] A. J. Hodge , J. A. Petruska. *Recent studies with the electron microscope on ordered aggregates of the tropocollagen molecule. In Aspects of Protein Chemistry (G. N. Ramachandran, Ed.),*. Academic Press, London, 1963.

[23] M. P. Wenger , L. Bozec ,M. A. Horton , P. Mesquida. Mechanical properties of collagen fibrils. *Biophysical journal*, 93:1255–1263, 2007.

[24] R. Bruce Bach , David Burr , Neil A. Sharkey. *Skeletal Tissue Mechanics pages 151*. Springer Science+Business Media, 1998.

[25] J. Khoshnoodi, J.-P. Cartailler, K. Alvares, A. Veis, , and B. G. Hudson. Molecular recognition in the assembly of collagens: terminal noncollagenous domains are key recognition modules in the formation of triple helical protomers. *Journal of Biological Chemistry*, 281(50):38117–38121, 2006.

[26] Claire Pigault. Osmose-pression osmotique 2010 `http://unt-ori2.crihan.fr/unspf/2010_Strasbourg_Pigault_Osmose/co/00_Module_Osmose_web.html`.

[27] R. B. Svensson , T. Hassenkam , P. Hansen, S. P. Magnusson. Viscoelastic behavior of discrete human collagen fibrils. *Journal of the Mechanical Behavior of Biomedical Materials 3*, pages 112–115, 2010.

[28] M. J. Buehler. Nature designs tough collagen: Explaining the nanostructure of collagen fibrils. *PNAS*, 103(33):12285–12290, 2006.

[29] L. Bozec and M. Horton. Topography and mechanical properties of single molecules of type i collagen using atomic force microscopy. *Biophysical journal*, 88(6):4223–4231, 2005.

[30] YL. Sun, ZP. Luo, A. Fertala, and KN. An. Stretching type ii collagen with optical tweezers. *journal of Biomechanics*, 37(11):1665–1669, 2004.

[31] C.A. Grant, D.J Brockwell, S.E Radford, and N.H Thomson. Tuning the elastic modulus of hydrated collagen fibrils. *Biophysical journal*, 97(11):2985–2992, 2009.

[32] S. Leikin, D.C Rau, and V.A Parsegian. Temperature-favoured assembly of collagen is driven by hydrophilic not hydrophobic interactions. *Nat. Struct. Mol. Biol.*, 2:205–210, 1995.

[33] R.B. Svensson, T. Hassenkam, C.A. Grant, and S.P. Magnusson. Tensile properties of human collagen fibrils and fascicles are insensitive to environmental salts. *Biophysical Journal*, 99:4020–4027, 2010.

[34] Davide Ricci, Pier Carlo Braga. *Recognizing and avoiding artifacts in afm imaging (in Atomic Force Microscopy)* . Springer, 2004.

[35] JPK Instrument. *JPK NanoWizard II - User Manual*. 2010.

[36] Chemwiki. Lennard-jones potential `http://chemwiki.ucdavis.edu/Physical_Chemistry/Physical_Properties_of_Matter/Intermolecular_Forces/Lennard-Jones_Potential`.

[37] W.Richard Bowen, Nidal Hilal. *Atomic force microscopy in process engineering*. Elsevier, 2009.

[38] John E. Sader, James W. M. Chon, and Paul Mulvaney. Calibration of rectangular atomic force microscope cantilevers. *Review of Scientific Instruments*, 70(10):3967–3969, 1999.

[39] JPK Instruments. Summary notes - force spectroscopy measurements and processing. Technical report, JPK Instruments, 2009.

[40] O. G. Andriotis, S. W. Chang, M. Vanleene, P. H. Howarth, D. E. Davies, S. J. Shefelbine, M. J. Buehler, and P. J. Thurner. Structure–mechanics relationships of collagen fibrils in the osteogenesis imperfecta mouse model. *Journal of The Royal Society Interface*, 12(111), 2015.

[41] H. Bueckle, J. Westbrook, and H. Conrad. *The Science of Hardness Testing and its Research Applications.* American Society for Metals ,MaterialsPark, Ohio., 1973.

[42] W. C. Oliver , G. M. Pharr. Measurement of hardness and elastic modulus by instrumented indentation: Advances in understanding and refinements to methodology. *Journal of materials research 19*, pages 3–20, 2004.

[43] M. Loparic , D. Wirz , A. Daniels , R. Raiteri , M. R. VanLandingham , G. Guex , I. Martin , U. Aebi , M. Stolz. Micro-and nanomechanical analysis of articular cartilage by indentation-type atomic force microscopy: validation with a gel-microfiber composite. *Biophysical journal 98*, pages 2731–2740, 2010.

[44] C. A. Grant , D. J. Brockwell , S. E. Radford , N. H. Thomson. effects of hydration on the mechanical response of individual collagen fibrils. *Applied Physics Letters*, 92:233902–233902, 2008.

[45] M. A. Hopcroft , W. D. Nix , T. W. Kenny. What is the young's modulus of silicon? *Journal of Microelectromechanical Systems 19*, pages 229–238, 2010.

[46] R. Puxkandl , I. Zizak , O. Paris , J. Keckes , W. Tesch , S. Bernstorff , P. Purslow , P. Fratzl. Viscoelastic properties of collagen: sunchrofron radiation investigations and structural model. *Phil Trans Roy Soc London B*, 357:191–197, 2002.

[47] Blake Erickson, Ming Fang, Joseph M. Wallace, Bradford G. Orr, Clifford M. Les, and Mark M. Banaszak Holl. Nanoscale structure of type i collagen fibrils: Quantitative measurement of d-spacing. *Biotechnology journal*, 8:117–126, 2013.

[48] Joseph M. Wallace, Qishui Chen, Ming Fang, Blake Erickson, Bradford G. Orr, and Mark M. Banaszak Holl. Type i collagen exists as a distribution of nanoscale morphologies in teeth, bones, and tendons. *Langmuir*, 26(10):7349–7354, 2010.

[49] J.M. Veres, S.P and. Harrison and Michael Lee J. Mechanically overloading collagen fibrils uncoils collagen molecules, placing them in a stable, denatured state. *Matrix biology*, 33:54–59, 2014.

[50] Lasse Ryhänen, Edward J. Zaragoza, and Jouni Uitto. Conformational stability of type i collagen triple helix: Evidence for temporary and local relaxation of the protein conformation using a proteolytic probe. *Biochemistry and Biophysics*, 223:562–571, 1983.

[51] J. Peltonen, N.J. Cronin, L. Stenroth, T. Finni, and J. Avela. Viscoelastic properties of the achilles tendon in vivo. *SpringerPlus*, 2, 2013.

[52] W. C. Herrick , H. B. Kingsbury , D. Y. S. Lou. A study of the normal range of strain, strain rate, and stiffness of tendon. *Journal of biomedical materials research 12*, pages 877–894, 1978.

[53] B. M. Nigg , B. R. Maclintosh , J. Mester. *Biomechanics and Biology of Movement - Chapter Mechanical effects of forces.* Human Kinetics Publishers, 2000.

[54] K.W. Hinchcliff, A.J Kaneps, and Geor R.J. *Equine Exercise Physiology: The Science of Exercise in the Athletic Horse.* Elsevier Health Sciences., 2008.

[55] P. Fratzl , K. Misof , I. Zizak , G. Rapp , H. Amenitsch , S. Bernstorff. Fibrillar structure and mechanical properties of collagen. *Journal of Structural Biology 122*, pages 119–122, 1998.

[56] K. L. Ong , S. Lovald , J. Black. *Orthopaedic Biomaterials in Research and Practice, Second Edition - Chapter Properties of natural materials.* CRC Press, 2014.

[57] M. Nordin , V. H. Frankel. *Basic Biomechanics of the Musculoskeletal System - Chapter 4 Biomechanics of tendons and ligaments.* Fourth edition, 2012.

[58] R. Peter Rand. Osmotic pressure data `https://www.brocku.ca/researchers/peter_rand/osmotic/osfile.html`.

[59] Constantinos N. Maganaris. Tendon conditioning: artefact or property? *Proceedings of the Royal Society of London B: Biological Sciences*, 270(Suppl 1):S39–S42, 2003.

[60] M. Cardinale , R. Newton , K. Nosaka. *Strength and Conditioning: Biological Principles and Practical Applications.* Wiley-Blackwell, 2011.